sustainability

MDPI

Article

Long-Term Stochastic Co-Scheduling of Hydro–Wind–PV Systems Using Enhanced Evolutionary Multi-Objective Optimization

Bin Ji [1], Haiyang Huang [1], Yu Gao [1], Fangliang Zhu [2], Jie Gao [3], Chen Chen [3], Samson S. Yu [4] and Zenghai Zhao [2,*]

[1] School of Traffic & Transportation Engineering, Central South University, Changsha 410075, China; cumtjibin@126.com (B.J.); haiyanghuang@csu.edu.cn (H.H.); 234211039@csu.edu.cn (Y.G.)
[2] China Water Resources and Hydropower Construction Engineering Consulting Co., Ltd., Beijing 100120, China; zhufl_zy@powerchina.cn
[3] China Renewable Energy Engineering Institute, Beijing 100120, China; gaojie@creei.cn (J.G.); hhy_ahut@163.com (C.C.)
[4] School of Engineering, Deakin University, Geelong 3216, Australia; s.yu@ieee.org
* Correspondence: chenchen1@creei.cn

Abstract: With the increasing presence of large-scale new energy sources, such as wind and photovoltaic (PV) systems, integrating traditional hydropower with wind and PV power into a hydro–wind–PV complementary system in economic dispatch can effectively mitigate wind and PV fluctuations. In this study, Markov chains and the Copula joint distribution function were adopted to quantize the spatiotemporal relationships among hydro, wind and PV, whereby runoff, wind, and PV output scenarios were generated to simulate their uncertainties. A dual-objective optimization model is proposed for the long-term hydro–wind–PV co-scheduling (LHWP-CS) problem. To solve the model, a well-tailored evolutionary multi-objective optimization method was developed, which combines multiple recombination operators and two different dominance rules for basic and elite populations. The proposed model and algorithm were tested on three annual reservoirs with large wind and PV farms in the Hongshui River Basin. The proposed algorithm demonstrates superior performance, with average improvements of 2.90% and 2.63% in total power generation, and 1.23% and 0.96% in minimum output expectation compared to BORG and NSGA-II, respectively. The results also infer that the number of scenarios is a key parameter in achieving a tradeoff between economics and risk.

Keywords: hydro–wind–PV co-scheduling; long-term stochastic scheduling; Markov chains; Copula joint distribution; multi-objective optimization

check for updates

Academic Editor: Gilles Notton

Received: 31 December 2024
Revised: 27 February 2025
Accepted: 28 February 2025
Published: 3 March 2025

Citation: Ji, B.; Huang, H.; Gao, Y.; Zhu, F.; Gao, J.; Chen, C.; Yu, S.S.; Zhao, Z. Long-Term Stochastic Co-Scheduling of Hydro–Wind–PV Systems Using Enhanced Evolutionary Multi-Objective Optimization. *Sustainability* **2025**, *17*, 2181. https://doi.org/10.3390/su17052181

Copyright: © 2025 by the authors. Licensee MDPI, Basel, Switzerland. This article is an open access article distributed under the terms and conditions of the Creative Commons Attribution (CC BY) license (https://creativecommons.org/licenses/by/4.0/).

1. Introduction

As global economies and populations continue to grow, the increasing demand for energy sharply contrasts with the limitations and non-renewable nature of traditional fossil fuel-based energy sources [1]. This conflict is further exacerbated by global climate change, making the resolution of this issue an urgent matter. It has become the primary driving force behind global energy structural adjustments, with the development and utilization of renewable energy standing at the core of the solution. Increasing the penetration of clean and renewable energy sources such as photovoltaic (PV), wind, geothermal, hydro, wave, and tidal energy into conventional power systems is crucial [2,3]. However, renewable energy sources like wind and PV are subject to weather conditions, exhibiting intermittent, random, and fluctuating characteristics, which pose significant threats to the secure and

stable operation of the power grid [4]. To fully harness the flexibility of hydropower and the natural complementarities between different energy sources, complementary generation has become an effective approach to promoting the integration of renewable energy. This has emerged as a key focus of international research in the fields of power systems and energy in recent years [5]. Currently, common multi-energy complementary systems include hydro–PV complementary systems [6], hydro–wind complementary systems [7], and hydro–wind–PV complementary systems [8]. Research on multi-energy complementary systems mainly focuses on three aspects: the configuration of generator capacity [9], the complementary characteristics of hydropower and wind–PV energy [10], and the operational scheduling of multi-energy complementary systems [11].

In the field of multi-energy complementary system operation scheduling, significant research progress has been made internationally in the area of short-term complementary operation scheduling [12,13]. The primary focus has been on short-term power output forecasting of energy sources such as wind and PV, the characterization of output uncertainty, the construction of short-term complementary scheduling optimization models, and the design of efficient solution algorithms [2]. Wang et al. [14] proposed a short-term joint scheduling model that takes into account the strategy of variable speed units and the principle of minimum number of start-up units, aiming to effectively cope with the regulatory deficiencies of traditional hydro–wind–PV complementary systems. Zhang et al. [15] studied the optimization of multi-time scale operations and ultra-short-term energy storage and distribution to meet the challenges of hydropower integration with wind and photovoltaic, achieving overall optimization in the long, medium and short term. Among the various forecasting models, methods such as linear/non-linear regression, support vector machines, frequency domain decomposition, deep learning, and combinations of these approaches have been employed. However, the accuracy of wind and PV energy forecasting remains insufficient to meet the practical requirements for real-world applications [16]. To address this, scholars have used techniques like stochastic distribution, scenario sets, confidence intervals, and fuzzy functions to characterize the uncertainty of wind and PV power output [8,17,18]. To address uncertainty in resource inputs, three primary approaches have emerged: (i) statistical distribution based on historical data; (ii) generating scenarios through methods like Monte Carlo simulations or extended Latin hypercube sampling and reducing them to typical scenarios; and (iii) using machine learning to predict based on historical data. In recent studies, uncertainty in long-term runoff and the output of wind and PV energy sources has been quantified through the use of coupled scenario sets generated by combining extended Latin hypercube sampling with k-means clustering reduction techniques [8] Furthermore, Luo et al. [18] considers the forecast errors in wind and PV power generation by treating the forecasted generation errors for each time period as independent normal distributions. These errors are then divided into multiple intervals for statistical fitting using piecewise methods, in conjunction with the aforementioned scenario analysis techniques. However, the approach of generating a large number of samples through stochastic simulations and applying scenario reduction does not account for the correlation characteristics between resources in the actual scheduling process. To address this, the Copula function has been widely applied, as it allows for the connection of cumulative distribution functions of variables with the same marginal distribution, thus accommodating the need to consider dependencies between resources [19]. To better understand the complementary mechanisms of hydropower, wind, and PV resources under multiple uncertainties, Camal et al. [20] used a full nesting method along with the asymmetric Archimedean Copula (AAC) based on the maximum likelihood function. Additionally, two Copula-based methods have been proposed for simulating the uncertainty of hydropower–wind–PV resources. The “Direct Gaussian” method con-

structs a multivariate time-dependent model between total production variables to derive the cumulative distribution function of total output. In contrast, the "Indirect Gaussian" method, instead of directly predicting total output, predicts individual energy sources and simulates the dependencies between different energy productions across various sectors, using the "Indirect Vine" method to generate scenarios. In [21], a large number of scenarios are first generated using extended Latin hypercube sampling, considering eight candidate marginal distributions commonly used in hydrological literatures. The best-fitting marginal distribution is selected, followed by the construction of a joint probability distribution using two common Archimedean Copulas: the Clayton Copula and the Frank Copula. The aforementioned studies primarily focus on the temporal correlations between different resources. This study, however, will further explore the potential spatial correlations between runoff and wind–PV output within the same watershed, arising from their geographical proximity.

Research on the long-term scheduling of multi-energy complementary systems is relatively limited. However, in the real-world cascading reservoir scheduling, long-term plans need to be formulated for the annual reservoirs. In the long term, runoff is a prominent uncertainty factor that cannot be accurately predicted, making it a highly challenging issue. Meanwhile, long-term scheduling better captures the seasonal fluctuations and variability of renewable energy sources such as hydropower, wind, and PV, which are influenced by changing environmental conditions. Due to the non-dispatchability of wind and PV power, the multi-energy complementary scheduling problem essentially revolves around reservoir scheduling under the boundary conditions of renewable energy integration. Building upon traditional hydropower scheduling frameworks, scholars have made valuable preliminary explorations by considering the complementary operational characteristics of different energy sources [18,22,23]. By transforming the multi-stage long-term operation process into a two-stage operation problem including the current stage and the reserve stage, Ding et al. [24] overcame the challenge of forecast uncertainty to cascade reservoir reserve and optimized the long-term operation of the hydro–wind–PV hybrid system. In order to effectively integrate large-scale renewable energy in the electricity market, Xu et al. [25] developed an operational model of water-solar complementary power generation systems that takes into account long-term electricity prices. Zhang et al. [26] considered the different interests of energy storage stations and intelligent buildings to achieve a win-win situation with uncertain electricity prices. These studies mainly focus on the extraction of long-term scheduling rules [22], multi-scale model nesting [23], and multi-objective scheduling optimization [4,26,27]. Some scholars have employed stochastic optimization scheduling methods and parameter simulation optimization approaches, proposing long-term optimization scheduling rules for hydro-PV complementary power stations based on scheduling principles, scheduling diagrams, and scheduling functions [5]. Such studies are often based on deterministic optimization models for scheduling, falling under the category of implicit stochastic scheduling. Therefore, other researchers have adopted explicit stochastic optimization scheduling frameworks, developing hydro-PV complementary stochastic programming models to analyze the impact of considering PV output uncertainty on improving the performance of complementary scheduling [28]. This study adopts the latter approach, utilizing stochastic scheduling. In addition, scholars have developed long-term optimization scheduling models for hydro–PV complementary systems with objectives such as maximizing power generation [8], achieving the highest generation guarantee rate [29], and minimizing the water shortage index [30]. These traditional single-objective optimization scheduling solutions often fail to guarantee relative optimality in other objectives, particularly when there is no clear trade-off between different objectives or when the objectives are in conflict. Therefore, another important research direction for the long-term scheduling of multi-energy complementary systems is multi-objective

optimization, considering goals such as maximizing power generation [31], ensuring the highest generation guarantee rate [31], minimizing the standard deviation of residual load [8], and reducing the overall risk rate [4]. Furthermore, risk assessment methods like Conditional Value-at-Risk (CVaR) [32] enhance long-term hydro–wind–PV scheduling by mitigating extreme uncertainties. Integrating CVaR into stochastic optimization models penalizes high-risk scenarios, leading to robust strategies that balance economic goals with operational reliability, thus avoiding over-optimism and guaranteeing feasibility in real-world conditions. This study addresses two critical challenges in renewable energy system operations through the LHWP-CS model: (i) the uncertainties in renewable resource generation, and (ii) transmission capacity limitations. In traditional methods, the spatio-temporal relationships between uncertainties of runoff, wind power and PV power have not been fully considered, which is usually investigated as Markov chains on time series. In light of this, we propose a scenario-based stochastic optimization framework that explicitly incorporates the temporal variability and spatial intermittency of hydro, wind, and PV power. Unlike conventional deterministic models, our approach enables more accurate and adaptive long-term power scheduling by reflecting real-world uncertainties. Additionally, we integrate transmission network constraints into the model, ensuring operational feasibility and grid stability under variable generation conditions—an often-overlooked aspect in current scheduling methodologies. The dual-objective optimization function balances the maximization of expected power generation with the minimization of power deficits, addressing the trade-off between efficiency and system reliability.

The techniques for multi-objective mathematical program can be classified into four categories according to the timing of preference information articulation versus the optimization [33]: (i) prior articulation of preferences such as the lexicographic goal programming and achievement scalarizing function approach [34,35], (ii) progressive articulation of preferences, (iii) posterior articulation of preferences, and (iv) a combination of two or more of the approaches above. For various techniques, the effort required in solving a multi-objective mathematical program for the decision maker is quite different. A key drawback of prior approaches, such as the weighted sum method, is the difficulty of specifying the required preference information. In this study, we adopt the method with posterior articulation of preferences, which finds all (or most) of the solutions for different scenarios rather than assigning weights to the objective functions. To achieve this, multi-objective optimization algorithm is proposed for solving the dual-objective optimization model, where the conflict between the two objectives is handled by the Pareto dominance and ε-box dominance rules.

Overall, research on the long-term scheduling of multi-energy complementary systems has made significant strides and produced results that offer valuable insights. However, several key challenges remain unresolved. These include (i) how to comprehensively consider the correlations between renewable energy sources during the long-term multi-energy complementary scheduling process, in order to more accurately characterize their multiple uncertainties; (ii) how to effectively construct models for the long-term stochastic scheduling of hydropower, taking into account the dynamic changes and uncertainties of hydropower resources; and (iii) how to improve the robustness of multi-objective optimization methods across different scheduling scenarios. To address the aforementioned challenges, this study employs Markov chains and Copula joint distribution functions to quantify the spatiotemporal correlations among hydro, wind, and PV energy sources. By generating scenarios for runoff, wind, and PV output, we simulate the associated uncertainties. Based on the characterization of these uncertain scenarios, we propose a bi-objective optimization model targeted at LHWP-CS. To solve this model, a customized evolutionary multi-objective optimization method is introduced. Furthermore, a decision-

making method from [36] is applied to further analyze the long-term scheduling plans, and short-term adjustments are made to the output based on resource complementarity characteristics. The main contributions of this study are summarized as follows:

1. Based on historical information and statistical laws, a C-vine model of pair-Copula is constructed by combining Markov chains with Copula functions, to quantitatively analyze the temporal correlation of runoff, wind power, and PV energy in cascaded watersheds, as well as the correlation among these resources. The runoff scenarios are then processed using Copula functions to ensure that the generated runoff scenarios adhere to the normal operation rules of cascaded reservoirs. Thereafter, scenario generation and reduction methods are employed to reasonably describe the multidimensional uncertainties.
2. Based on the stochastic characteristics of hydro, wind, and PV power, a multi-objective stochastic scheduling optimization model for cascade hydropower plants is developed, with various hydraulic constraints and other generation-related constraints, such as the transmission capacity, considered, aiming at maximizing expected total power generation and expected minimum output in each period.
3. An improved evolutionary multi-objective optimization method is proposed to solve the optimization model for LHWP-CS, incorporating key techniques such as a dominance rule fusion mechanism, multi-population fusion mechanism, and various heuristic constraint handling strategies. The algorithm efficiently solves large-scale multi-objective optimization problems and outperforms the comparisons.

The remainder of this paper is organized as follows: Section 2 presents the analysis of multi-fold uncertainties; Section 3 introduces the proposed long-term multi-objective scheduling model, including the objective functions and constraints for LHWP-CS. Section 4 describes the solution algorithm, including the proposed algorithm, heuristic adjustment strategies, and short-term correction mechanisms. Section 5 presents the research area, experimental results, and discussion. Section 6 concludes and provides recommendations for future applications.

2. Analysis of Uncertainties in the LHWP-CS Problem

The runoff, wind, and PV resources exhibit non-stationary temporal dynamics, and there are significant differences in the correlation between resources in different geographical locations. The state transition matrix of Markov chain provides an intuitive temporal dynamic explanation, without requiring the assumption of time-series stationarity, compared to Auto Regressive Integrated Moving Average (ARIMA) [37]. The Copula function allows for flexible selection of edge distributions and Copula types, effectively characterizing spatial heterogeneity and nonlinear tail correlations. Compared with deep learning models, Copula functions have more relaxed sample size requirements and are suitable for scenarios with limited historical data on water, wind, and PV [38]. Combining two methods—Markov chain for temporal dimension and Copula for spatial dimension—can simultaneously meet the requirements of spatiotemporal modeling [39]. However, it is difficult to consider spatial statistical models or pure time-series models simultaneously. Therefore, this study chooses to jointly model and analyze the spatiotemporal correlation of runoff, wind, and PV resources using a Markov chain and the Copula function.

2.1. Time Correlation Analysis of the Runoff, Wind, and PV Power

In order to characterize the seasonal characteristics of hydropower, wind power, and PV energy, an appropriate time correlation model is constructed in this study.

Specifically, historical data are divided into T units by month, denoted by μ, where $\mu \in \{1, \ldots, T\}$. Since the modeling processes for runoff, wind power, and PV output are

the same, the following takes runoff as an example to elaborate on the specific steps of model construction.

Step 1: Based on the monthly runoff data within the study area, each unit is divided into s states according to the transition patterns between months, totaling $s \times \mu$ state intervals.

Step 2: Based on the state transition intervals divided in Step 1, calculate the state transition probability matrix P^{runoff} for runoff, where the sum of probabilities in each row is 1.

$$P^{runoff} = \begin{pmatrix} P_{1,1} & P_{1,2} & \cdots & P_{1,s} \\ P_{2,1} & P_{2,2} & \cdots & P_{2,s} \\ \vdots & \vdots & \ddots & \vdots \\ P_{s,1} & P_{s,2} & \cdots & P_{s,s} \end{pmatrix} \tag{1}$$

This matrix is composed of different state transition probabilities $P_{i,j}$, as follows

$$P_{i,j} = P(\alpha_{t+1} = j | \alpha_t = i) = \frac{f_{i,j}}{\sum_{j=1}^{s} f_{i,j}} \tag{2}$$

where α_{t+1} and α_t represent the states of runoff in months t and t+1, respectively, and $f_{i,j}$ is the frequency of runoff transitioning from state i to state j, with $i, j \in s$.

Step 3: Based on the transition frequency matrix obtained in Step 2, we calculate the cumulative transition frequency matrix Q^{runoff} for runoff.

$$Q^{wind} = \begin{pmatrix} q_{1,1} & q_{1,2} & \cdots & q_{1,s} \\ q_{2,1} & q_{2,2} & \cdots & q_{2,s} \\ \vdots & \vdots & \ddots & \vdots \\ q_{s,1} & q_{s,2} & \cdots & q_{s,s} \end{pmatrix} \tag{3}$$

In the above formula, $q_{i,j} = \sum_{k=1}^{j} p_{i,k}$.

2.2. Correlation Analysis Among Runoff, Wind, and PV Power

Due to spatial proximity, there also exists correlation among heterogeneous resources such as runoff and the output of wind and PV power within the same river basin. To describe the correlation among these three variables, a mixed Copula distribution function is selected to construct a C-vine model [40,41] for analysis. Taking runoff as an example, the specific steps for model construction are presented below:

Step 1: Define the runoff, wind power output, and PV power output as random variables, and fit the marginal distribution of each variable using a non-parametric kernel density estimation method.

Step 2: Determine the vine structure by calculating the Kendall's tau coefficient between each pair of variables and maximizing the absolute value of the Kendall's tau coefficient. The formula for calculating Kendall's correlation coefficient is:

$$\tau = P\left[(X - X')(Y - Y') > 0\right] - P\left[(X - X')(Y - Y') < 0\right] \tag{4}$$

where $P(\cdot)$ is the probability distribution function, and the random vectors (X, Y) and (X', Y') follow the same distribution.

Step 3: Based on the vine structure determined in step 2, estimate the parameters of each Copula function using the maximum likelihood method. Then, use the AIC criterion to determine the Copula function for each edge by selecting the Copula function with the

smallest AIC value. This completes the construction of the C-vine model with Copula functions connected accordingly.

2.3. Generation of Uncertainty Scenarios

Before generating scenario sets that consider the uncertainties of runoff, wind power, and PV resources, it is necessary to first generate scenario sets that consider temporal correlation. The main idea is to first construct a Markov chain model following the above steps, and then use Monte Carlo sampling to generate scenario sets with temporal correlation. Based on this, the final scenario set of runoff, wind power, and PV power can be generated, which takes into account the correlation among these heterogeneous resources. The specific steps are as follows:

Step 1: Select the variable with the largest absolute sum of Kendall's tau coefficients with other variables to generate scenarios considering temporal correlation. The corresponding cumulative probability of this variable is denoted as the uniform variable Z_1, where $Z_1 \in [0, 1]$.

Step 2: Let U_1, U_2, and U_3 be three sets of variables to be solved. Set U_1 equal to the variable obtained in step 2, i.e., $U_1 = Z_1$. Z_1 can be regarded as the sample point for solving variable U_1.

Step 3: Generate two random numbers that follow a uniform distribution, defined as uniform variables Z_2 and Z_3. According to the obtained C-vine Copula model and the conditional distribution function $F(x|v)$, the second set of variables to be solved, U_2, can be calculated using $Z_2 = F(x_2|x_1) = \partial C(U_1|U_2)/\partial U_1$, where both Z_2 and U_1 are known quantities. This transforms the problem into a unary linear equation solving problem. In this study, the bisection method is used to solve the equation, and the solution obtained is the sample point for the variable to be solved, U_2.

Step 4: Similarly, since Z_2 and Z_3 have already been defined, we can derive $F(x_3|x_1)$ from $Z_3 = F(x_3|x_1, x_2) = \partial C_{x_3,x_2|x_1}(F(x_3|x_1, Z_2)/\partial Z_2$. Furthermore, $F(x_3|x_1) = \partial C(U_1|U_3)/\partial U_1$. By solving this equation, the result obtained is the sample point for the variable to be solved, U_3.

Step 5: Finally, perform inverse transform sampling on U_1, U_2, and U_3 to convert the aforementioned random samples into a final scenario set that considers both temporal correlation and the correlation between heterogeneous energy sources.

2.4. Reduction in Uncertainty Scenarios

To enhance computational efficiency and accuracy, this study adopts a scenario reduction technique [42] based on probabilistic distance to decrease the number of scenarios, achieving a high-quality approximation of the initial scenarios with a limited number of scenarios. The basic steps of synchronous back substitution elimination are as follows:

Step 1: Determine the probability of each original scenario as $1/M$.

Step 2: Calculate the probabilistic distance between each pair of scenarios, and the scenario with the smallest probabilistic distance is the one that needs to be eliminated.

Step 3: Adjust the total number of scenarios and the corresponding probabilities: Set the total number of scenarios M to $M - 1$, and add the probability of the eliminated scenario to the nearest remaining scenario to ensure that the sum of the probabilities of the retained scenarios is 1.

Step 4: If the total number of remaining scenarios M is greater than the specified number of scenarios to retain, return to step 2, and repeat until the number of scenarios is reduced to the specified number.

3. Mathematical Model for the LHWP-CS Problem

Based on the obtained runoff and wind–PV output stochastic scenarios, a long-term stochastic multi-objective optimization model for the LHWP-CS problem is proposed. The model established in this study focuses on decision-making in the power generation of hydro–wind–PV systems with various hydraulic-related constraints considered, while some factors that may exist in practice such as power demand fluctuation and market price fluctuation are ignored.

3.1. Decision Variables

In this study, the discharge flow $QT_{n,t}$ of hydropower plant n at time period t is taken as the decision variables of the model.

3.2. Objective Functions

Two objectives are set for the model to maximize the total power generation of the whole scheduling period (i.e., (5)) and expected minimum output in each period (i.e., (6)). Let the set of scenarios for runoff, wind power, and PV outputs be denoted by J, with the scenario probability p_j. The objective function used can be described as follows,

$$\text{Max } F = \left(\sum_{n\in N} \sum_{j\in J} \sum_{t\in T} P_{n,j,t}.p_j + \sum_{j\in J} \sum_{t\in T} P_{j,t}^{wind}.p_j + \sum_{j\in J} \sum_{t\in T} P_{j,t}^{solar}.p_j \right) \Delta T - \sum_{k\in K} \sum_{j\in J} w_k \left(\delta_{j,k}^{-} + \delta_{j,k}^{+} \right) \quad (5)$$

where T represent the set of long-term scheduling periods, and N denote the set of hydropower plants. $P_{n,j,t}$ refers to the output of hydropower plant n at time period t under the j runoff scenario. $P_{j,t}^{wind}$ represents the output of the wind turbines at time period t under the j scenario, and $P_{j,t}^{solar}$ represents the output of the PV units at time period t under the j scenario. ΔT denotes the length of the long-term scheduling period. $\delta_{j,k}^{-}$, $\delta_{j,k}^{+}, k = \{1, 2, .., 6\}$, $j \in \{1, 2, \ldots, |J|+1\}$ represent the degree of constraint violation when the corresponding constraint is insufficient or exceeded, and w_k is the penalty factor associated with the k constraint. Here, $|J|$ denotes the number of scenarios. The total output of the system at time t, denoted as P_t, is expressed as follows,

$$P_t = \text{Max}_{t\in T} \left[\sum_{j\in J} P_{j,t}^{wind}.p_j + \sum_{j\in J} P_{j,t}^{solar}.p_j + \sum_{n\in N} \sum_{j\in J} P_{n,j,t}.p_j \right]^{min} - \sum_{k\in K} \sum_{j\in J} w_k \left(\delta_{j,k}^{-} + \delta_{j,k}^{+} \right). \quad (6)$$

3.3. Constraints

(1) Water balance of reservoirs:

$$V_{n,j,t+1} = V_{n,j,t} + I_{n,j,t} + \sum_{m\in\Omega(n)} QT_{m,t} - QT_{n,t}, \ \forall n \in N, \ t \in T, \ j \in J \quad (7)$$

where $V_{n,j,t+1}, V_{n,j,t}$ represent the reservoir storage of hydropower plant n at long-term periods $t+1$ and t, respectively. Term $I_{n,j,t}$, denotes the inflow of hydropower plant n at time period t, and $\Omega(n)$ represents the set of upstream reservoirs of reservoir n. Term $QT_{n,t}$ represents the discharge flow of hydropower plant n at time period t, which satisfies the following constraint.

$$QT_{n,t} = QP_{n,t} + S_{n,t}, \forall n \in N, t \in T \quad (8)$$

where $QP_{n,t}, S_{n,t}$ represent the power generation flow and the spillage flow of hydropower plant n at time period t, respectively.

(2) Discharge flow limit:

$$\underline{QT_{n,t}} \le QT_{n,t} + \delta^{-}_{|J|+1,1} + \delta^{+}_{|J|+1,1} \le \overline{QT_{n,t}}, \forall n \in N, t \in T \tag{9}$$

where $\underline{QT_{n,t}}$ and $\overline{QT_{n,t}}$ represent the lower and upper bounds of the total discharge flow of hydropower plant n at time period t, respectively.

(3) Generation flow limit:

$$\underline{QP_{n,t}} \le QP_{n,t} + \delta^{-}_{|J|+1,2} + \delta^{+}_{|J|+1,2} \le \overline{QP_{n,t}}, \forall n \in N, t \in T \tag{10}$$

where $QP_{n,t}$ and $\overline{QP_{n,t}}$ represent the lower and upper bounds of the power generation flow of hydropower plant n at time period t, respectively.

(4) Output limit:

$$\underline{P_{n,t}} \le P_{n,j,t} + \delta^{-}_{j,3} + \delta^{+}_{j,3} \le \overline{P_{n,t}}, \forall n \in N, t \in T, j \in J \tag{11}$$

where $\underline{P_{n,t}}$ and $\overline{P_{n,t}}$ represent the lower and upper bounds of the power generation of hydropower plant n at time period t, respectively; $P_{n,j,t}$ denotes the output of hydropower plant n at time period t under the j runoff scenario.

(5) Storage limit:

$$\underline{V_{n,t}} \le V_{n,j,t} + \delta^{-}_{j,4} + \delta^{+}_{j,4} \le \overline{V_{n,t}}, \forall n \in N, t \in T, j \in J \tag{12}$$

where $\underline{V_{n,t}}$ and $\overline{V_{n,t}}$ represent the lower and upper bounds of the reservoir storage of hydropower plant n at time period t, respectively.

(6) Water level constraints at the beginning and end of dispatching period:

$$Z_{n,j,1} = Z_{n,Ini}, \forall n \in N, j \in J \tag{13}$$

$$Z_{n,j,T} + \delta^{-}_{j,5} + \delta^{+}_{j,5} = Z_{n,End}, \forall n \in N, j \in J \tag{14}$$

where $Z_{n,Ini}$, $Z_{n,End}$ represent the initial and final water levels of hydropower plant n, respectively.

(7) Water level–storage relationship:

$$V_{n,j,t} = f^{zy}_{n}\left(Z_{n,j,t}\right), \forall n \in N, t \in T, j \in J \tag{15}$$

where $f^{zy}_{n}(\cdot)$ is the nonlinear function representing the relationship between water level and storage for the reservoir.

(8) Tailwater level–outflow relationship:

$$Z^{d}_{n,j,t} = f^{down}_{n}(QT_{n,t}), \forall n \in N, t \in T, j \in J \tag{16}$$

where $f^{down}_{n}(\cdot)$ is the nonlinear function relating the tailwater level to the outflow discharge of station n, and $Z^{d}_{n,j,t}$ is the tailwater level of station n during time t under the j runoff scenario.

(9) Hydropower generation function:

$$H_{n,j,t} = \frac{Z_{n,j,t+1} + Z_{n,j,t}}{2} - Z^{d}_{n,j,t}, \forall n \in N, t \in T, j \in J \tag{17}$$

$$P_{n,j,t} = K_n.H_{n,j,t}.QP_{n,t}, \forall n \in N, t \in T, j \in J \tag{18}$$

where $H_{n,j,t}$ is the hydraulic head for station n during time t under the j runoff scenario, and K_n is the power generation coefficient of station n.

(10) Transmission capacity constraints:

$$\sum_{i \in W_n} F_i + \sum_{j \in B_n} F_j + F_n + \delta^{-}_{|J|+1,6} + \delta^{+}_{|J|+1,6} \leq TC_n^{max}, \forall i \in W_n, j \in B_n, n \in N \quad (19)$$

where W_n and B_n are the sets of wind and PV power plants associated with station n, F_n, F_i, and F_j are the outputs of hydro, wind, and PV power plants, respectively, and $TC_n^{\max}$ is the maximum integrated hydro-wind-PV transmission capacity of station n.

4. Solution Method for the LHWP-CS Problem

The LHWP-CS model is highly non-linear due to the hydropower generation function and other nonlinear constraints. The economic dynamic dispatch problem for hydro plants is proven to be a NP-hard problem [43]. Integrating the uncertain nature of the wind and PV power makes the LHWP-CS problem difficult to optimally solve. In order to obtain satisfactory solution for the problem within reasonable computational resources, heuristic algorithms should be designed. To address these challenges, an evolutionary-based multi-objective optimization algorithm is proposed based on the Borg algorithm(EBORG), which was proposed for multi-objective optimization benchmarks in [44,45].

The Borg algorithm introduces a basic population and elite population which are updated according to Pareto-dominance and $\epsilon - box$ dominance rules. Meanwhile, multiple candidate recombination operators are integrated and operators with better performance are given higher priority for selection. The algorithm combines multiple recombination operators and two dominance rules, whereas traditional algorithms often implement a single recombination operator and one dominance rule (known as the Pareto-dominance rule). The adaptive multi-method search framework enhances the robustness of algorithm for solving problems under different scenarios [46]. In contrast to the traditional methods that use Pareto-dominance rule, the integrated $\varepsilon - box$ dominance rule enhances the convergence ability of algorithm and the diversity of solutions [44]. In the standard Borg algorithm, a solution in the archive population is substituted randomly if any of the following conditions are met: (i) the solution is randomly chosen when it is dominated by a new solution according to the $\epsilon - box$ dominance rule, (ii) the solution is randomly chosen when it is non-dominated with a new solution. This strategy undermines the convergence and diversity of the new generated archive population, which could be improved by introducing $\epsilon - box$ dominance ranking and crowding distance criteria. The framework of the improved Borg algorithm is illustrated in Figure 1, and key techniques are introduced in the following text.

4.1. Population Coding

The individuals in the population corresponding to multiple scenarios for a single set of decision variables are encoded as follows. The individual encoding can be described as:

$$X_i = \{QT_{11}, \ldots, QT_{1T}, \ldots, QT_{NT}\} \quad (20)$$

where N represents the number of cascade hydropower plants and T is the total number of long-term scheduling periods. The encoding represents the discharge flow $QT_{n,t}$ of hydropower plant n at time period t, which is randomly generated within a specified range.

4.2. Multi-Dominance Rule Fusion Strategy

In this study, both the base population and the elite population are designed, as shown in Figure 1. The base population is selected using the Pareto dominance rule, while the elite population is selected using the $\epsilon - box$ dominance ranking and crowding distance rule. A brief introduction to these two dominance rules is provided below.

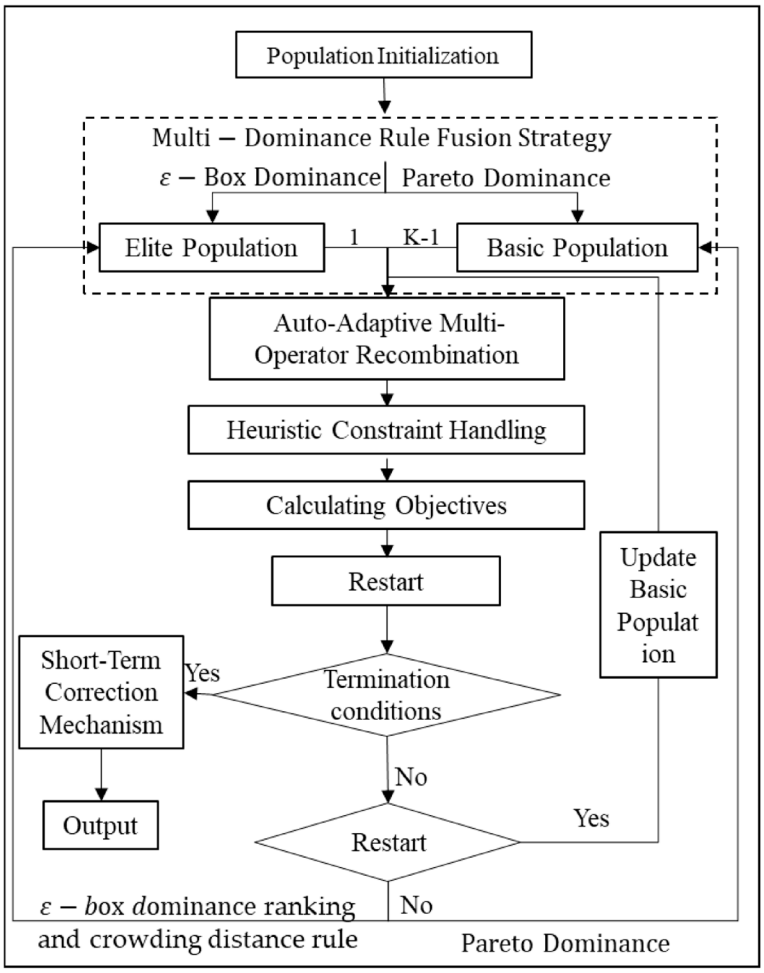


Figure 1. Flowchart of the optimized algorithm for LHWP-CS.

4.2.1. Pareto Dominance Rule

Theorem 1. *In a multi-objective optimization problem model aimed at minimizing an objective function, for two vectors* $\boldsymbol{u}$ *and* $\boldsymbol{v}$ *in the decision space, the vector* $\boldsymbol{u}$ *is said to dominate vector* $\boldsymbol{v}$ *(denoted as* $\boldsymbol{u} \prec \boldsymbol{v}$*) if the following two conditions are satisfied:*

(i) The value of each objective function in vector $\boldsymbol{u}$ *is no greater than the corresponding objective function value in vector* $\boldsymbol{v}$*, meaning that the optimization results of all objective functions in vector* $\boldsymbol{u}$ *are at least as good as those in vector* $\boldsymbol{v}$*;*

(ii) There exists at least one objective function in vector $\boldsymbol{u}$ *that is strictly smaller than the corresponding objective function value in vector* $\boldsymbol{v}$*, indicating that at least one optimization result in vector* $\boldsymbol{u}$ *is better than that in vector* $\boldsymbol{v}$*.*

4.2.2. The Proposed $\epsilon - box$ Dominance Ranking and Crowding Distance Rule

The $\epsilon - box$ dominance is an extension of the $\epsilon - dominance$ rule [44]. The $\epsilon -$ dominance is defined as follows:

Theorem 2. *For a given* $\epsilon > 0$*, a vector* $\boldsymbol{u} = (u_1, u_2, \ldots, u_M)$ $\epsilon - dominates$ *another vector* $v = (v_1, v_2, \ldots, v_M)$ *if and only if:*

For $\forall i \in \{1, 2, \ldots, M\}, u_i \leq v_i + \epsilon$*, and* $\exists j \in \{1, 2, \ldots, M\}, u_j < v_j + \epsilon$*.*

The $\epsilon - box$ *dominance set is defined for a given* $\epsilon > 0$*, such that vector* $\boldsymbol{u} = (u_1, u_2, \ldots, u_M)$ $\epsilon - box$ *dominates another vector* $v = (v_1, v_2, \ldots, v_M)$ *if at least one of the following conditions is satisfied:*

$$(i) \quad \left\lfloor \frac{u}{\epsilon} \right\rfloor \prec \left\lfloor \frac{v}{\epsilon} \right\rfloor$$
$$(ii) \quad \left\lfloor \frac{u}{\epsilon} \right\rfloor = \left\lfloor \frac{v}{\epsilon} \right\rfloor \;\&\; \| u - \left\lfloor \frac{u}{\epsilon} \right\rfloor \| < \| v - \left\lfloor \frac{v}{\epsilon} \right\rfloor \|$$

This relationship is denoted as $u \prec_{\in} v$. The $\epsilon - box$ dominance operates by dividing each dimension of the objective space vector by a small ϵ, truncating the result to integers, and then applying Pareto dominance to the truncated vectors. This dominance relationship effectively divides the objective space into grids with ϵ as the side length, as illustrated in Figure 2a.

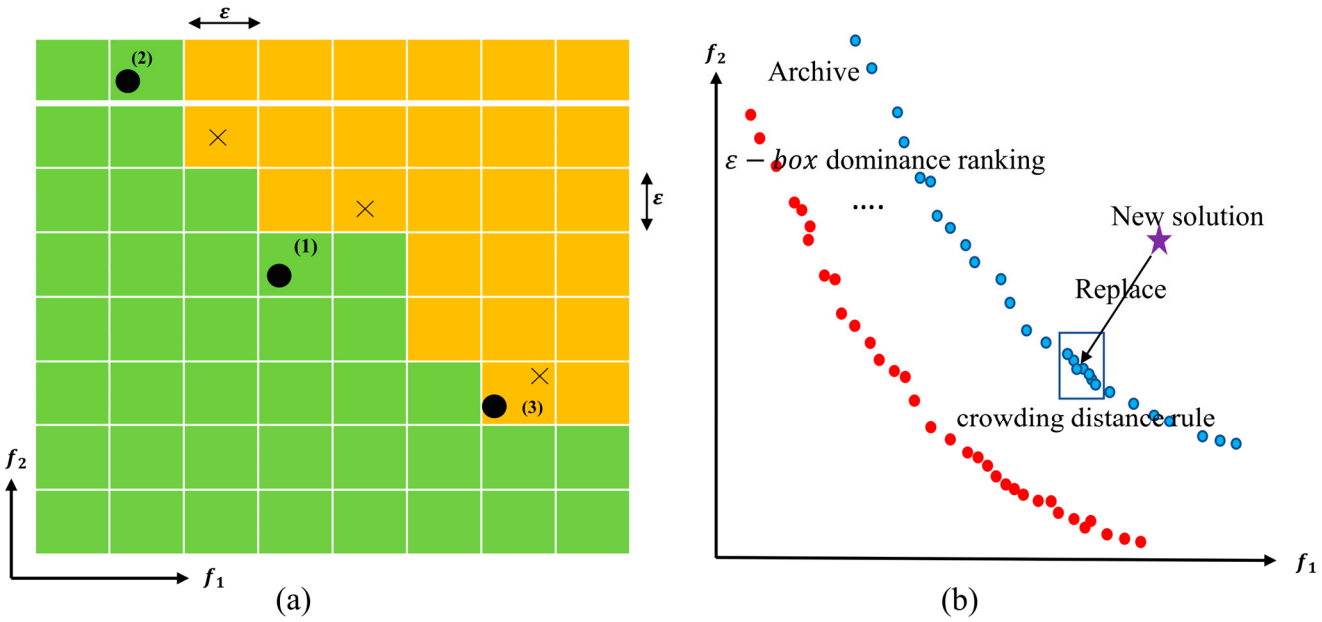


Figure 2. Illustration of the proposed rule: (**a**) $\epsilon - box$ dominance rule and (**b**) process of using the improved strategy (Red circles and blue circles represent the solution sets of different levels after sorting, and the stars represent new solutions.).

When the solutions are located in different grids, the comparison is made based on the $\epsilon - dominance$ relationship. When the solutions are in the same grid, the comparison uses the $\epsilon - box\ dominance$ to determine which point is closest to the central point (the top-right corner of the grid). In Figure 2a, the "×" symbol represents individuals in the dominated population, the new solutions to be added to the dominated population are indicated by black dots, and the yellow area represents the region dominated by the dominated population. A new solution will only be added to the dominated population if its performance improvement exceeds the threshold ϵ.

When Solution 1 and Solution 2 are added to the elite population, this process is part of the $\epsilon - dominance$, while adding Solution 3 to the elite population belongs to the $\epsilon - box$ dominance process. In this study, the two objective functions are the maximization of the expected total power output of the hydro–wind–PV complementary system and the minimization of the expected output. Let $u = \{F, P\}$, and then the aforementioned dominance relations can be applied to LHWP-CS.

This study proposes to replace the standard Borg algorithm's random update mechanism with an improved strategy based on $\epsilon - box$ dominance ranking and crowding distance [47]. This optimization approach aims to enhance the population's search and update mechanism. The update process consists of two steps to improve both the evolutionary performance of the population and the diversity of solutions as shown in Figure 2b:

First, when newly generated offspring dominate the population, $\epsilon - box$ dominance sorting is used to rank these superior solutions, and then randomly selected solutions from

the bottom of the ranking are replaced. This approach prevents high-quality solutions with potential convergence from being accidentally discarded, ensuring that the population gradually converges towards the optimal solution region while maintaining diversity.

Second, when the offspring solution does not dominate any existing solution in the population, the crowding distance for all solutions is calculated, and offspring replace the solution with the smallest crowding distance. This step effectively preserves the diversity of the population.

4.2.3. Auto-Adaptive Multi-Operator Recombination and Restart Mechanism

In this study, an auto-adaptive multi-operator recombination mechanism is adopted, abandoning the use of a single genetic recombination operator. Instead, a pool of multiple crossover operators is used, and a feedback mechanism is established to compare the performance of these operators during the search process. Operators that perform well will be assigned higher selection weights. Specifically, initially, all operators have equal selection weights, and their probabilities for selection in the next iteration are updated via the feedback mechanism. The selection criterion is the number of solutions in the elite population generated by an operator through $\epsilon - box$ dominance. Let M_i represent the performance of operator i, with the initial selection probabilities for the K crossover operators being equal. C_i represents the number of elite individuals generated by operator i; the larger the proportion of elite individuals generated, the higher the probability of selecting that operator.

$$M_i = \frac{(C_i + \varsigma)}{\sum_{j=1}^{K}(C_j + \varsigma)} \tag{21}$$

where the constant $\varsigma > 0$ is used to prevent the operator probability from reaching zero, thereby ensuring that no operator is "lost" during the execution of the algorithm. The specific crossover operators selected for this algorithm are referenced from [45].

A prominent feature of the EBORG algorithm's multi-population fusion is the introduction of an elite population. To avoid the algorithm getting trapped in local optima, a population restart mechanism [44] is designed to detect stagnation in the algorithm's search. If stagnation is detected, the restart mechanism is triggered to regenerate the base population. This mechanism adaptively adjusts the population size and updates the base population individuals, enabling the algorithm to reinitiate the search process when stagnation or local optima are encountered, in order to find better solutions. The size of the restarted population is determined based on the size of the elite population in the optimization process of the LHWP-CS. Let γ represent the ratio of the base population size to the elite population size. After the restart mechanism is triggered, the base population size is calculated according to the current size of the elite population and the ratio γ. The base population is cleared, and the elite population individuals are used to refill it. Any remaining individuals are generated through mutations of the elite population.

4.3. Heuristic Constraint Handling Strategy

In the LHWP-CS model, the constraints will be handled by integrating two constraint-handling strategies. During the problem-solving process, the generation of initial solutions is random and may not necessarily satisfy the constraint conditions. These initial solutions are then incorporated into the constraint conditions, with a feasible solution priority strategy serving as the foundation for the preliminary search. Subsequently, a heuristic adjustment strategy is applied to improve the solution quality, thereby enhancing the search efficiency.

4.3.1. Feasible Solution Priority Strategy

The principle of the feasible solution priority strategy is to retain feasible solutions in the population as much as possible, based on the following three rules:

(i) If both solutions are feasible, selection is based on the Pareto dominance rule;
(ii) If one solution is feasible and the other is infeasible, the feasible solution is given priority;
(iii) If both solutions are infeasible, selection is made based on the degree of constraint violation.

4.3.2. Heuristic Adjustment

Due to the coupling nature of different constraints, any change in one variable within the model can trigger a chain reaction. Therefore, how to handle the constraints in the model is a key issue. Additionally, since the initial and final water levels of each reservoir are predetermined, the total discharge of each dam within a scheduling cycle can be easily determined. One strategy is to first ensure that the water balance constraint is satisfied during each time interval, and then, without violating the water balance, correct the reservoir storage by adjusting the outflow. This is referred to as the neighboring time period heuristic repair strategy, where the core idea is to make adjustments at the micro level of neighboring time periods, thereby ensuring feasibility on a macro level. This approach represents a process that moves from local adjustments to global feasibility. For the coupled constraints involved in this study, Algorithm 1 will be used to handle the dynamic water balance constraint, and Algorithm 2 will be used to handle the reservoir storage capacity constraint [48]. The model will ensure that the water balance constraint is satisfied at each time interval. If the water storage exceeds the constraint, the volume exceeding the limit is first calculated, and then the discharge flow of the reservoir in that time period is adjusted based on the violation magnitude, so that the reservoir storage returns within the feasible range.

Algorithm 1: Dynamic Water Balance Regulation

Input: Reservoir discharge flow $QT_{n,t}$, Reservoir capacity constraints
Output: Optimized outflow
1. Calculate the water volume difference $\Delta QT_{n,t}$ for reservoir n at each period
2. FOR each period $t \in \Delta T$:
3. Adjusted flow $QT_{n,t} \leftarrow QT_{n,t} + \Delta QT_{n,t} \,/\, \Delta T$
4. IF $QT_{n,t} < \underline{QT_{n,t}}$: $QT_{n,t} \leftarrow \underline{QT_{n,t}}$
5. ELSE IF $QT_{n,t} > \overline{QT_{n,t}}$: $QT_{n,t} \leftarrow \overline{QT_{n,t}}$
6. Calculate new water volume difference $\Delta QT_{n,t}$
7. IF $\Delta QT_{n,t} = 0$:
8. End processing
9. ELSE:
10. Randomly select a scheduling period t
11. Adjust $QT_{n,t} \leftarrow QT_{n,t} + \Delta QT_{n,t} \,/\, \Delta T$
12. Apply flow range constraints:
13. IF $QT_{n,t} < \underline{QT_{n,t}}$: $QT_{n,t} \leftarrow \underline{QT_{n,t}}$
14. ELSE IF $QT_{n,t} > \overline{QT_{n,t}}$: $QT_{n,t} \leftarrow \overline{QT_{n,t}}$
15. IF $n \leq \Delta T$:
16. Counter $n \leftarrow n + 1$
17. Go back to Step 11
18. End processing

Algorithm 2: Reservoir Storage Regulation

Input: Reservoir storage $V_{n,j,t}$, Reservoir capacity constraints
Output: Adjusted discharge flow
1. Calculate the reservoir storage $V_{n,j,t}$ for each time period.
2. FOR each period $t \in \Delta T$:
3. IF $V_{n,j,t} < \underline{V_{n,t}}$ *OR* $V_{n,j,t} > \overline{V_{n,t}}$:
4. IF $V_{n,j,t} > \overline{V_{n,t}}$:
5. Calculate $\Delta V_{n,j,t} = \left(V_{n,j,t} - \overline{V_{n,t}}\right) / \Delta t$
6. Distribute $\Delta V_{n,j,t}$ evenly across the adjustment periods.
7. Transfer $\Delta V_{n,j,t}$ to adjacent reservoir outflows while respecting discharge flow constraints.
8. IF discharge flow > max allowable limit:
9. Calculate $\Delta V_1 = \Delta V_{n,j,t} - \left(V_{n,j,t} - \overline{V_{n,t}}\right)$
10. Distribute ΔV_1 across adjacent reservoirs to maintain maximum allowable discharge flow.
11. ELSE IF discharge flow < min allowable limit:
12. Calculate $\Delta V_1 = \Delta V_{n,j,t} - \left(\underline{V_{n,t}} - V_{n,j,t}\right)$
13. Adjust discharge flow to meet minimum allowable discharge level.
14. ELSE IF $V_{n,j,t} < \underline{V_{n,t}}$:
15. Calculate the shortfall $\Delta V_{n,j,t} = \left(\underline{V_{n,t}} - V_{n,j,t}\right) / \Delta t$
16. Distribute the shortfall $\Delta V_{n,j,t}$ evenly across the adjustment periods.
17. Transfer shortfall to adjacent reservoir outflows while respecting discharge flow constraints.
18. IF discharge low > max allowable limit:
19. Continue transferring to adjacent reservoirs to meet the maximum discharge flow limit.
20. ELSE IF discharge flow < min allowable limit:
21. Adjust discharge flow to meet minimum allowable discharge level.
22. END IF
23. Repeat until reservoir storage in all periods meets required range.
24. End processing.

4.4. Short-Term Correction Mechanism Based on Resource Complementarity

The short-term correction and adjustment of hydro–wind–PV resource complementarity are performed based on the obtained long-term power output and channel capacity. Specifically, wind and PV output power is superimposed on the hydropower output, and adjustments to the hydropower output are evaluated to determine whether optimization is feasible. The adjustments must comply with relevant basic principles, and the corrected and optimized outputs are defined on an hourly scale. The general correction methodology is described as follows:

(1) Basic Principles:

Considering the complementary characteristics of hydro, wind, and PV resources, the short-term correction mechanism adheres to the following three principles. The former principle has a higher priority to be satisfied.

(i) Adjusted output values must comply with transmission channel capacity limits.
(ii) Minimize water spillage.
(iii) Maximize the utilization of wind and PV energy.

(2) Short-term Correction Mechanism:

Based on the constructed model and developed algorithm, long-term scheduling plans are obtained, including reservoir water level trajectories and average power output. Assuming that hydropower plants operate according to their average output plans, the hourly hydropower output is denoted as P_{hydro}, and the actual wind and PV outputs are superimposed on the hydropower output. Due to transmission capacity constraints, it is necessary to check whether the total output exceeds the transmission channel capacity. The excess is calculated as $F = F_{total} - F_{channel}$, where:

$$F_{total} = \sum_{n \in N} \left(\sum_{i \in W_n} F_i + \sum_{j \in B_n} F_j + F_n \right), \quad F_{channel} = TC_n^{max} \tag{22}$$

For the portion exceeding the channel capacity ($\Delta F > 0$), the energy needs to be either curtailed or stored for later use, as shown in Figure 3a. The first correction mode takes the reservoir's average output as the hourly correction mode.

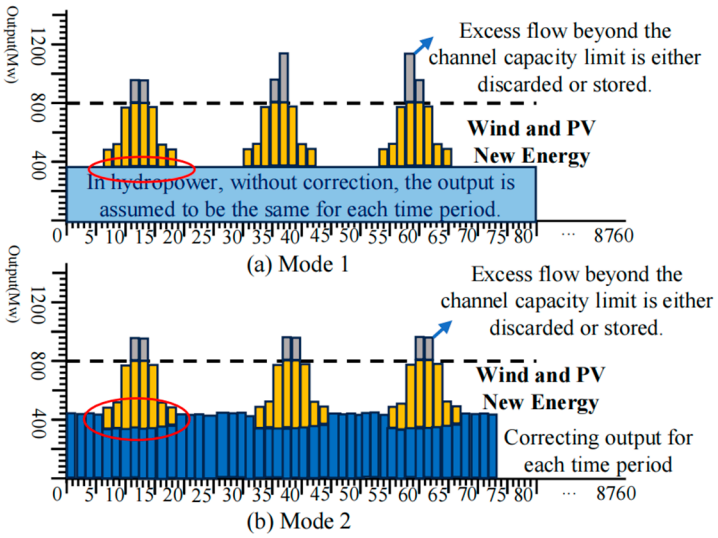


Figure 3. Illustration of the short-term correction mechanism.

In this study, the second correction mode, as shown in Figure 3b, is adopted. Hydropower output will not be directly scheduled based on the average output but will instead consider complementarity with wind and PV power. The basic principle is that during periods of high wind and PV output, hydropower can reduce its output accordingly. Conversely, during other time periods, hydropower output can be increased, enabling more efficient integration of wind and PV energy and enhancing the overall power generation of the system.

Specifically, optimization is assessed on the basis of the average output curve. In particular, the wind and PV output curve's peaks (referred to as "humps") are analyzed to determine whether the hydropower output can be reduced. For long-term scheduling scales, short-term corrections can be performed on an hourly basis, with daily time intervals treated cyclically. Wind and PV output periods are denoted as τ, and non-output periods are denoted as ς. Under the conditions of transmission channel capacity limits, the goal is to minimize hydropower output as much as possible. The amount of reduced power output is denoted as P_τ, and the reduced hydropower output is evenly distributed (i.e., P_τ/ς) across the rest of the curve, thus improving overall power generation efficiency. If reducing hydropower output results in water spillage, energy storage can be used to absorb wind and PV energy, further increasing the utilization of wind and PV power. The specific steps are outlined in Algorithm 3.

Algorithm 3: Short-Term Correction Mechanism

Input: long-term hydropower, wind and PV output power
Output: Optimized hourly hydro, wind and PV output power
1. Calculate the average hydropower;
2. FOR each hour ∈ scheduling period:
3. Total output ← Average hydropower + Wind and PV output
4. IF wind and PV output > 0:
5. IF average hydropower > minimum monthly average output level:
6. Reduction in output ← Average hydropower − (Total output − Wind and PV output)
7. FOR each hour ∈ scheduling period:
8. IF wind and PV output = 0:
9. Hydropower ← Hydropower − (Reduction in output/number of hours without output)
10. IF total output level > $TCmax$:
11. Handle excess situation (total output)
12. Output optimized (hydro, wind and PV output)

5. Case Study on Hongshuihe River

5.1. Introduction of the Case

The Hongshuihe River is one of China's twelve major hydropower bases, with 10 large-scale cascade hydropower stations, and large-scale wind and PV stations. In recent years, the Hongshui River basin has received extensive attention, and the combined development of hydropower and renewable energy has great demonstrative significance for promoting regional ecological balance and realizing sustainable development. Choosing the multi-energy system in this basin as a case study can not only reflect the practical application value, but also explore the theoretical innovation on hydro-wind-PV cooperative scheduling. The runoff data used in this case study are monthly-based and sourced from three hydropower stations along the Hongshuihe River: Tianshengqiao-I, Longtan, and Yantan, located, respectively, in the upstream, midstream, and downstream sections of the river. The selected time period covers from 1951 to 2010. The wind power and PV output data are hourly-based and represent the normalized data from a certain year of wind farms and PV plants in the Hongshuihe River basin. These normalized values are then multiplied by the installed capacities of the corresponding wind farms and PV plants to obtain the actual wind and PV output data. Other data are generated based on this foundation.

The fundamental data are provided in Table 1. Figure 4 illustrates the relationship between the three stations in the LHWP-CS.

Table 1. Basic Information of the study objects.

Name	Installed Capacity of Wind (MW)	Installed Capacity of PV (MW)	Installed Capacity of Hydro (MW)	Regulating Storage (Billion m^3)	Multi-Year Average Flow Rate (m^3/s)
TianshengqiaoI	360	1640	1200	5.796	579
Longtan	1230	7160	6300	11.2	1530
Yantan	620	2105	1810	0.425	1697

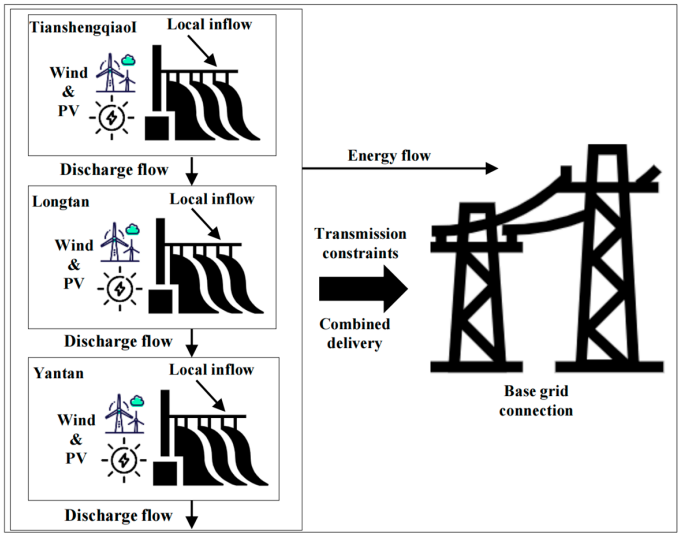


Figure 4. Schematic diagram of the hydro–wind–PV joint power generation system in the hongshui river basin.

5.2. Generation of Uncertainty Scenarios for Runoff, Wind, and PV Power

5.2.1. Time Correlation Analysis

Based on the runoff, wind, and PV data of the geographical area of interest, this paper divides each variable into four states and establishes the corresponding transition probability matrix and cumulative frequency transition matrix of the Markov chain according to the method described in Section 2.1. Some of the matrices obtained are shown in the following figures (taking the runoff of the Longtan hydropower station as an example).

As can be seen from Figures 5 and 6, taking runoff as an example, in most cases, the state of the previous month will transition to a certain state of the next month, which proves that a single variable of hydro, wind, and PV resources has temporal correlation.

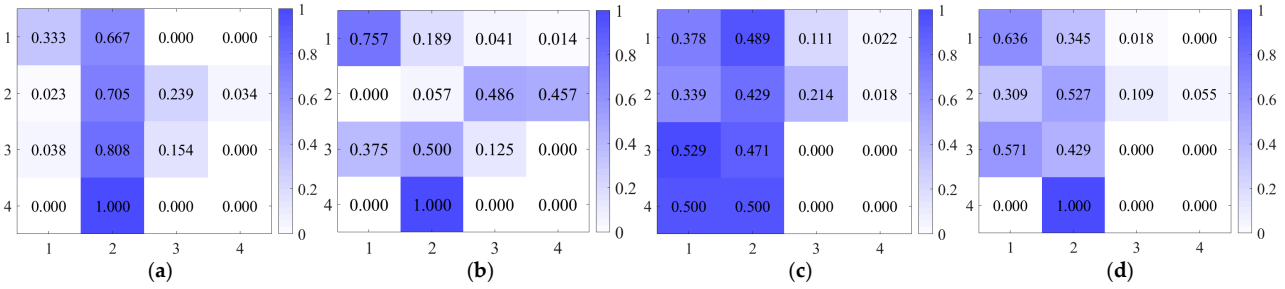


Figure 5. Transition probability matrix for runoff: (**a**) February and March; (**b**) May and June; (**c**) August and September; (**d**) November and December.

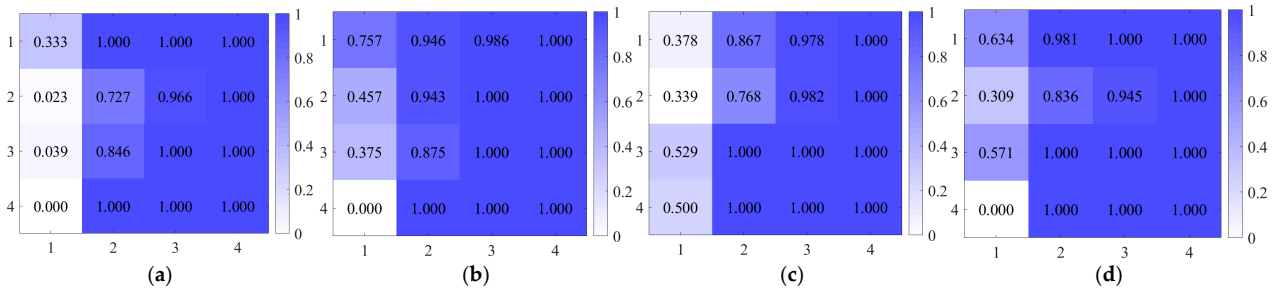


Figure 6. Cumulative transition frequency matrix for runoff: (**a**) February and March; (**b**) May and June; (**c**) August and September; (**d**) November and December.

5.2.2. Correlation Analysis Between Resources

Based on the copula distribution function discussed in Section 2.2, the correlation between water, wind, and PV resources is analyzed. First, the empirical distribution functions for each resource are calculated using the runoff data of the cascaded reservoirs and the power output data for wind and PV. A non-parametric estimation method is employed to determine the cumulative probability distributions of the three variables, as illustrated in Figure 7 (using the runoff of the Longtan Station as an example). Additionally, the power output data of wind and PV are calculated based on the installed capacity of the Longtan Station. Figure 7 demonstrates that the trend of curves is consistent, verifying that the non-parametric kernel density estimation method is effective for fitting the marginal distributions of each variable.

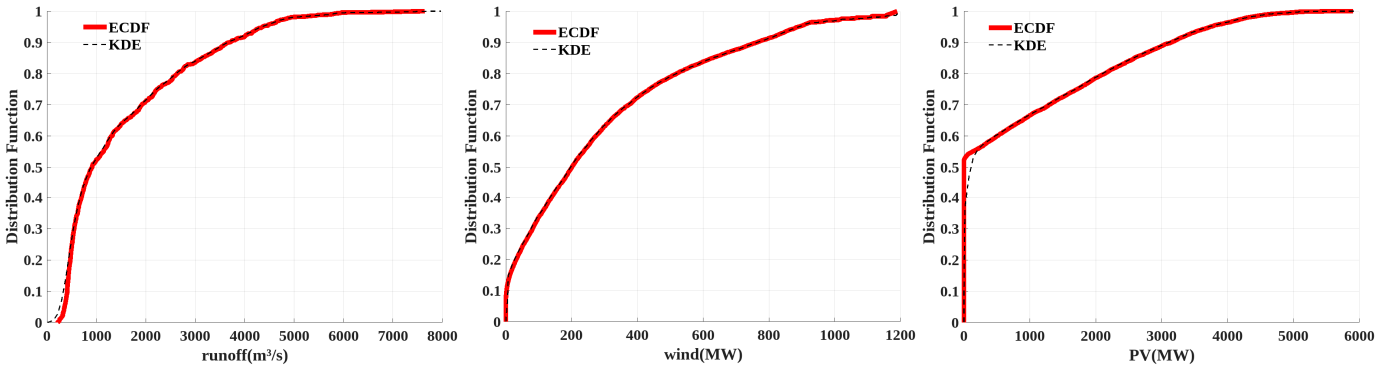


Figure 7. Marginal cumulative probability distribution function: (**a**) runoff; (**b**) wind; (**c**) PV.

Equation (4) is used to calculate the Kendall's tau coefficients between each pair of variables, and the results show that the Kendall's tau coefficients associated with PV output and runoff, PV output and wind power output are 0.455 and 0.576, respectively. A careful examination of the results finds that the sum of the Kendall's tau coefficients associated with PV output is larger than the other Kendall's tau coefficients associate with runoff and wind power output. In light of this, the PV variable is chosen as the central variable for the first layer. Suppose the runoff, wind power output, and PV output are represented by x_f, x_w, and x_p, respectively, the first-layer vine structure is composed of $x_w - x_p$ and $x_p - x_f$, while the second-layer vine structure forms a three-dimensional C-vine structure with $C_{p,w} - C_{p,f}$.

Then, the marginal distributions of X and Y are denoted as $U = F(x)$ and $V = G(y)$, respectively. In this study, five Copula functions (i.e., Gaussian Copula, t-Copula, Gumbel Copula, Clayton Copula, and Frank Copula) are used to estimate the linear correlation parameters and degrees of freedom. Subsequently, the Akaike Information Criterion (AIC) is applied to determine the most suitable Copula function for each margin. The specific results are presented in Table 2 (taking the Longtan Station as an example).

Table 2. AIC values for Copula functions on each edge of the C-vine structure.

	t Copula	Gaussian Copula	Gumbel	Clayton	Frank
$x_w - x_p$	−468.98	−415.26	2.01	2.00	−475.34
$x_p - x_f$	−12.46	1.73	1.99	−37.99	1.80
$C_{p,w} - C_{p,f}$	−7891.01	−783.34	−8045.40	−6103.62	−7441.37

In Table 2, a lower AIC value indicates a better model. Consequently, for the first layer of the C-vine model, the Frank Copula is selected for wind power output and PV output, with a parameter value of −1.7789. The Clayton Copula is selected for runoff and PV output, with a parameter value of 0.2511. For the second layer, the Gumbel Copula is chosen to characterize the correlation among hydro, wind, and PV resources, with a parameter value of 2.6015. The probability density functions of the respective Copula functions are illustrated in Figure 8.

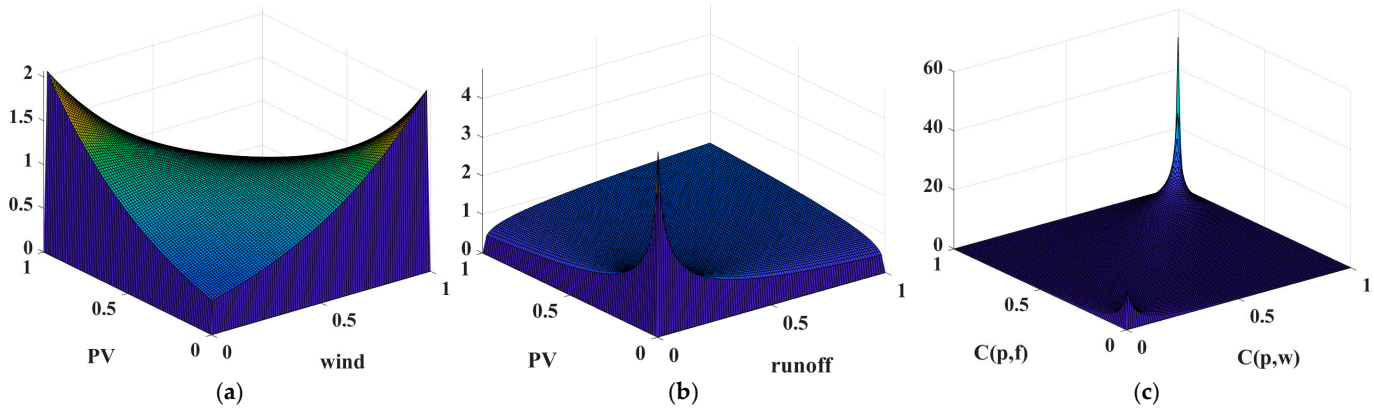


Figure 8. Probability density function for Copula function: (**a**) wind–PV; (**b**) wind–runoff; (**c**) wind–runoff–PV.

5.2.3. Generation of and Reduction in Uncertainty Scenarios

The hydropower station discussed in this study belongs to a cascaded reservoir system. Therefore, when generating runoff scenarios, it is necessary to consider the runoff flow correlation between upstream and downstream of the reservoir. To achieve this, the runoff of the upstream reservoir is taken as the initial input data, and the runoffs of the middle and downstream reservoirs can be obtained via the Copula function. Firstly, based on the Kendall coefficient calculation results in Section 5.2.2, the corresponding cumulative probabilities obtained by selecting the PV variable to generate time-correlated scenarios are denoted as Z_1, and the sample points U_1 for PV variables are obtained by letting $U_1 = Z_1$. Secondly, using the generated random number Z_2 and the copula conditional distribution function formula for wind power and PV, the sample points U_2 for wind power variables can be derived. Finally, based on the known random numbers Z_2 and Z_3, the upstream sample points U_3 for runoff are obtained by solving the Copula conditional distribution function formula for runoff and PV.

Subsequently, based on the principle of the Copula function, the data from TianshengqiaoI and Longtan are fitted using a Copula function as one group, and the data from Longtan and Yantan are fitted using a Copula function as another group. The most suitable copula function is selected using the AIC criterion, with the specific results shown in Table 3.

Table 3. AIC values calculation results for the Copula functions of the three hydropower stations.

	t Copula	Gaussian Copula	Gumbel	Clayton	Frank
TianshengqiaoI Longtan	−1356.79	−1329.30	−1251.13	−1166.08	−1344.14
Longtan–Yantan	−2989.98	−2884.24	−2983.39	−2323.96	−3084.32

According to the data in Table 3, the t-Copula function is selected for fitting between TianshengqiaoI and Longtan, with a parameter of 0.9213 and a degree of freedom of 5.8306.

The Frank Copula function is selected for fitting between Longtan and Yantan, with a parameter of 61.6272. Using the fitted Copula functions, the sample points of TianshengqiaoI obtained are taken as the input runoff data to sequentially obtain the runoff sample points of Longtan and Yantan. Then, inverse transform sampling is performed on the sample points of the three hydropower stations as well as the wind and PV sample points to obtain an uncertainty scenario set that considers the time correlation and correlation between heterogeneous resources for hydro, wind, and PV resources. Finally, the initial scenarios are reduced according to the scenario reduction method described in Section 2.4 to obtain the final scenario set for hydro, wind, and PV resources. The specific results are shown in Figure 9 (Taking TianshengqiaoI as an example).

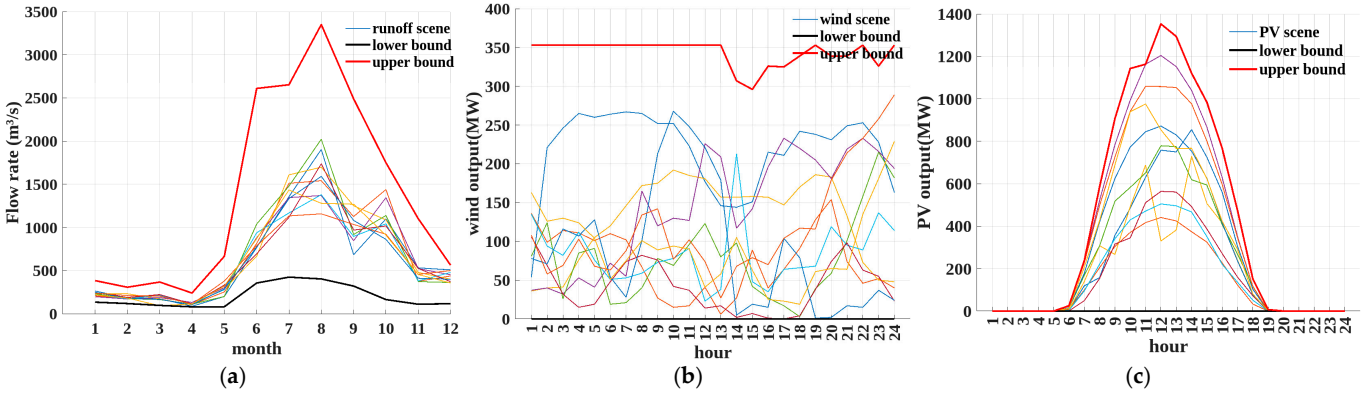


Figure 9. Uncertainty scenarios: (**a**) runoff; (**b**) wind output; (**c**) PV output.

It can be observed that the 10 scenarios all fall within the upper and lower limits of the initial scenarios, and show a good diversity.

5.3. Analysis of the Rationality of Model Solution Results

5.3.1. In a Single Scenario

The rationale of the solution method is investigated in a single scenario. The runoff, wind and PV input scenarios are shown in Figure 10, and the obtained Pareto front is shown in Figure 11. Figure 11 shows that the obtained Pareto frontier solutions are rich in diversity and evenly distributed, and there is an obvious mutually exclusive relationship between the two objective functions.

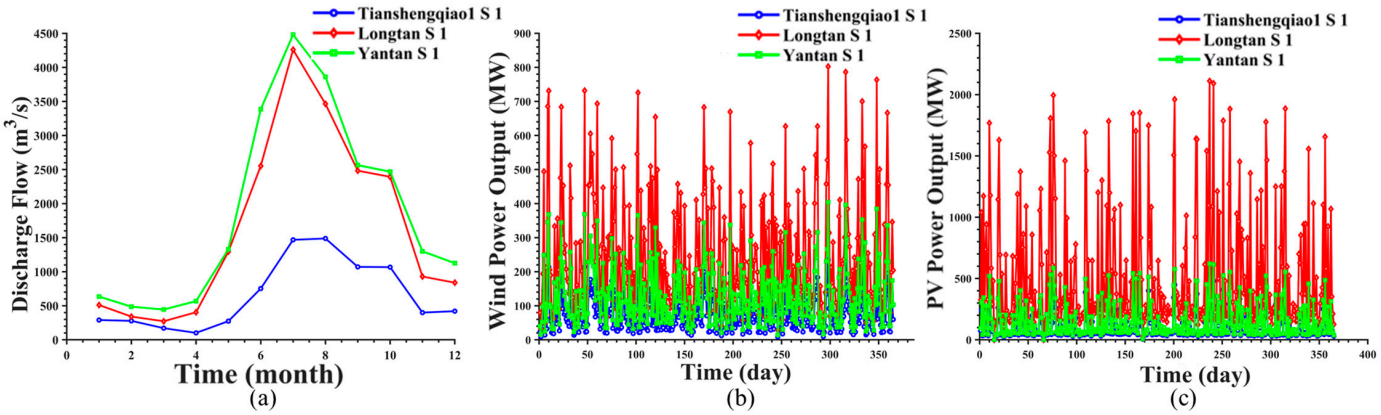


Figure 10. Input of each power station in a single scenario: (**a**) runoff, (**b**) wind power and (**c**) PV output.

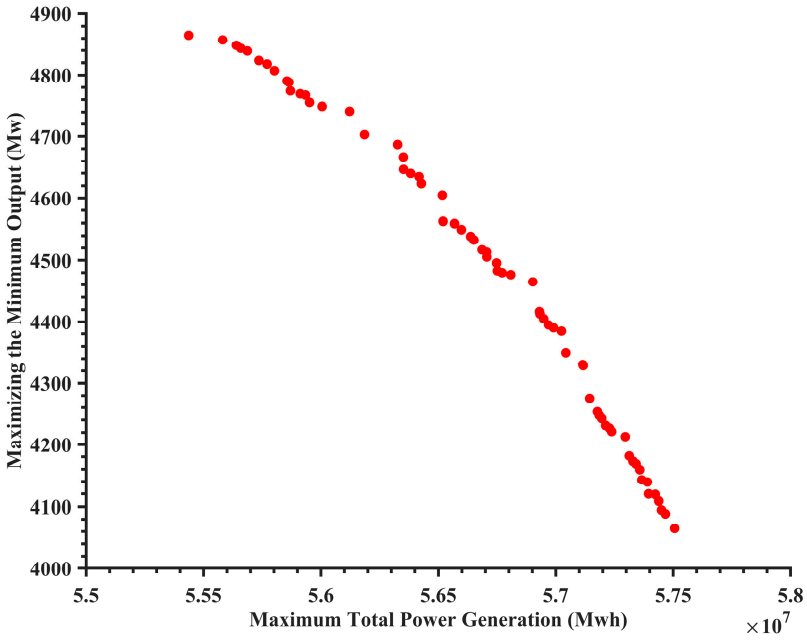


Figure 11. Pareto front solutions obtained in a single scenario.

Figures 12 and 13 illustrate the discharge flow, water level, and power output. The discharge flows, power generation flows, power outputs, and water level variations of TianshengqiaoI, Longtan, and Yantan hydropower stations all meet the boundary constraints, which infers the efficiency of the constraint handling strategies presented in this study. During the flood season, water spillage occurs at Yantan hydropower station. This is because the water level is strictly restricted at 219 m from May to August.

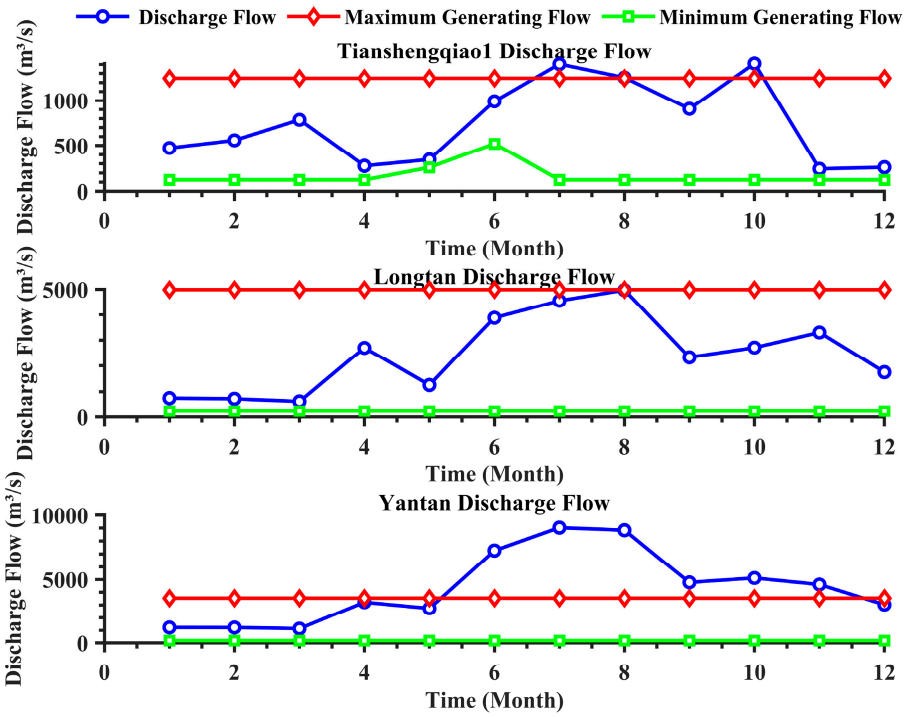


Figure 12. Discharge flows of each power station obtained under a single scenario.

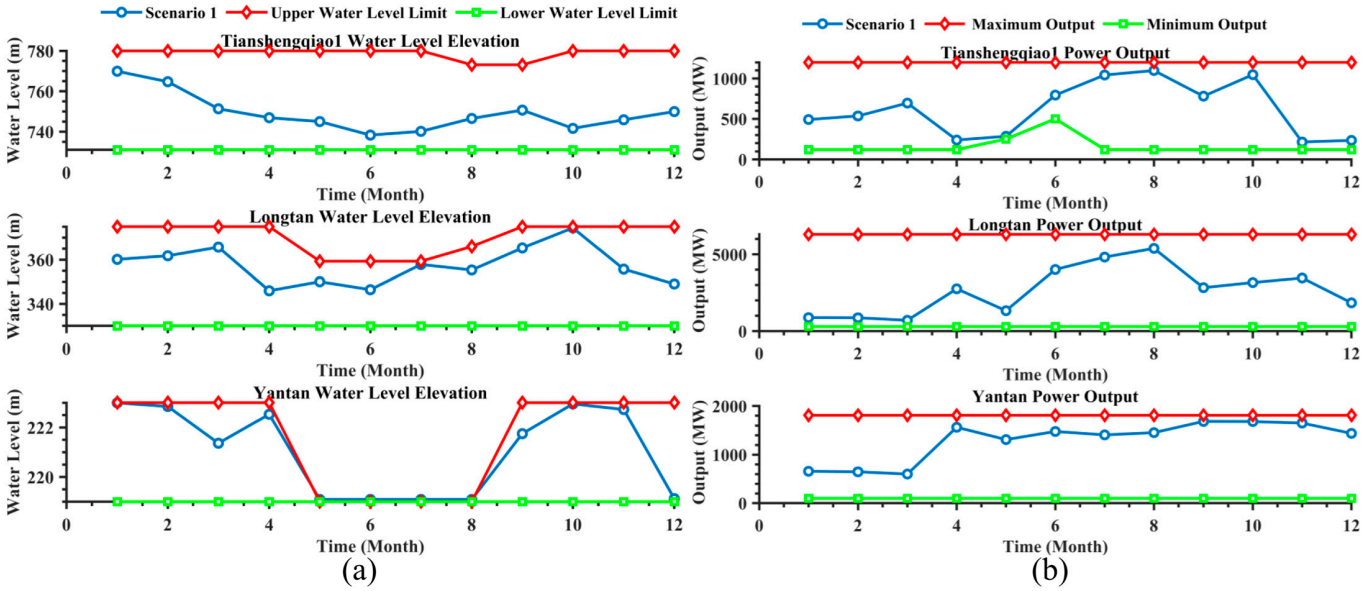


Figure 13. Water level, and power output of each power station obtained under a single scenario: (**a**) water level variation curves, (**b**) power output variation curves.

Figure 14 illustrates the hourly scale results obtained using the short-term correction mechanism (taking TianshengqiaoI as an example). In this figure, the gray and yellow sections represent the wind and PV power outputs superimposed on hydropower outputs, demonstrating the contribution of wind and PV resources to overall power generation. The results satisfy the transmission capacity constraints and reflect the characteristics of multi-energy complementarity. During the flood season from July to October, the average hydropower output is relatively high, highlighting the significant role of hydropower energy utilization during this period.

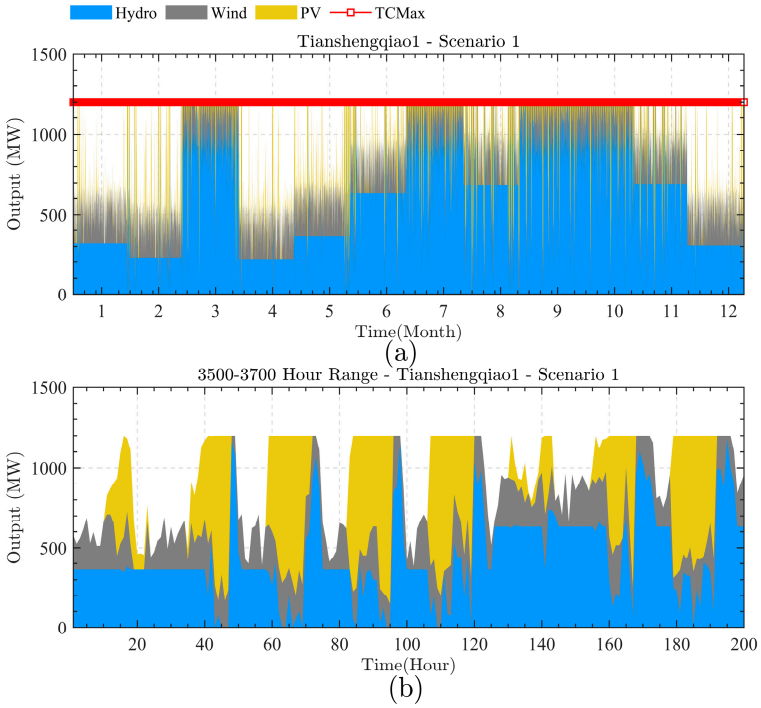


Figure 14. Short-term corrected hydro–wind–PV stacked power output chart for TianshengqiaoI in a single scenario: (**a**) stack plot shown by month and (**b**) local enlarged hourly stacking diagram.

5.3.2. In Multiple Scenarios

Furthermore, the solution method is tested under the configuration of five scenarios, with the runoff and wind/PV output in different scenarios shown in Figures 15–17.

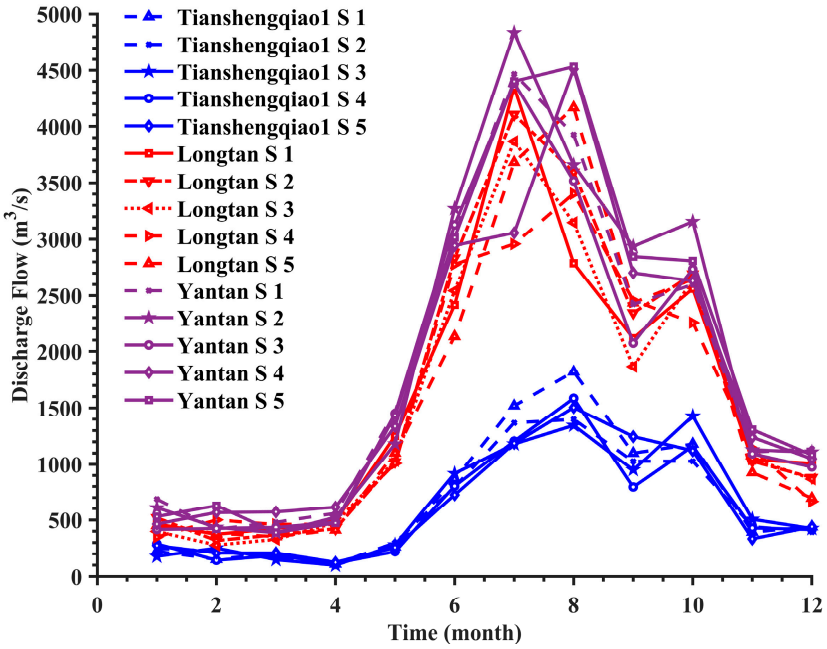


Figure 15. Runoff input of each power station in multiple scenarios.

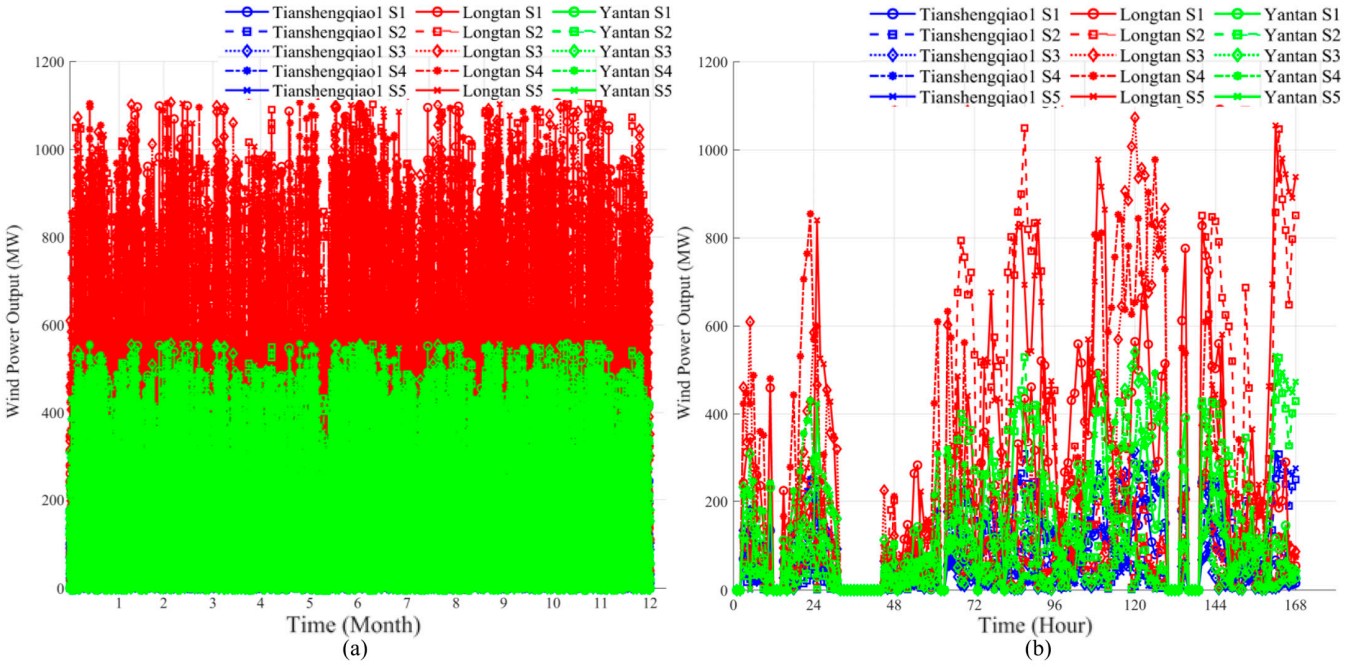


Figure 16. Wind power input of each power station in multiple scenarios: (**a**) line chart displayed by month and (**b**) partial magnification of first week.

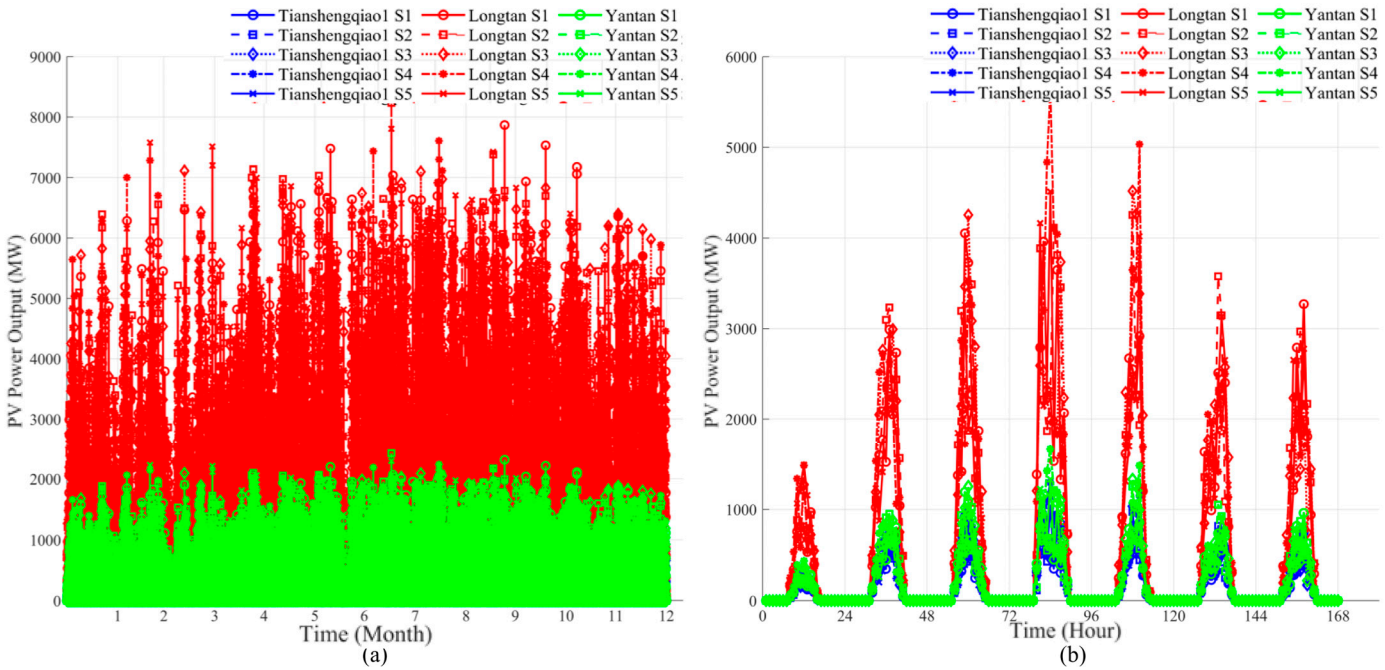


Figure 17. PV output of each power station in multiple scenarios: (**a**) line chart displayed by month and (**b**) partial magnification of first week.

The resulting Pareto fronts obtained under different number of scenarios are shown in Figure 18. It can be observed that the number of scenarios has significant impacts on the objective function values. As the number of scenario increases, both the total power generation and the minimal output in each month decrease. The results are consistent with the decision-making experience in practice. A larger number of scenarios means a wider range of values of runoff and wind and PV power outputs are considered in the model. The corresponding solution is more conservative, in order to lower the risk raised by the increasing number of scenarios. The results also infer that the number of scenarios is a key parameter in achieving a tradeoff between economic and risk.

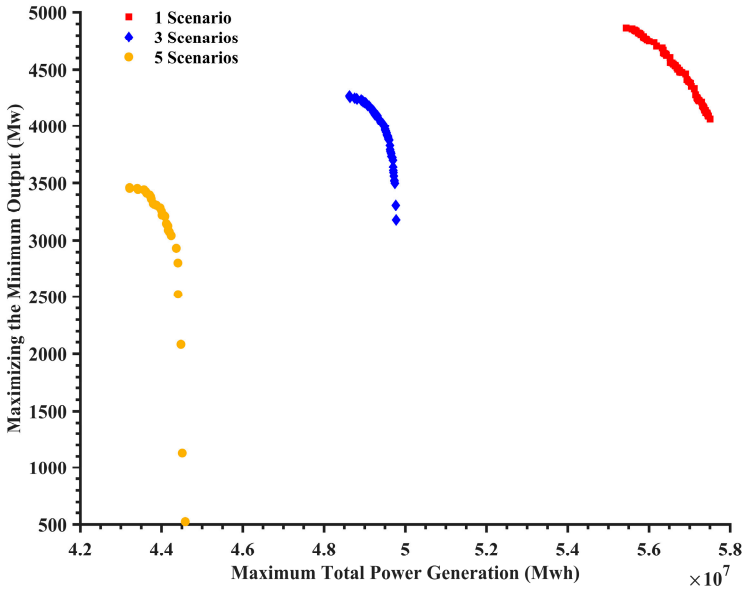


Figure 18. Pareto front solutions obtained in different scenarios.

Figures 19 and 20 show the discharge flows, water level and output for different scenarios. For the TianshengqiaoI and Longtan stations, there is no water spill. Meanwhile, and in all scenarios, the output and water levels meet the boundary constraints. During the flood season, water spill occurs at the Yantan station due to the head effect, leading to suboptimal generation. In most months, the water levels at Yantan meet the boundary constraints, except for some months between May to August. In the wet season from May to August, the water level at Yantan is strictly restricted to 219 m, resulting in the water level obtained under certain scenarios exceeding 219 m. The water level at TianshengqiaoI slightly decreases in the middle of the year and then rises. At the Longtan reservoir, the water level gradually increases through the year, reaching a peak before declining at the end of the year. The water level at Yantan exhibits relatively stronger fluctuations compared to the other stations.

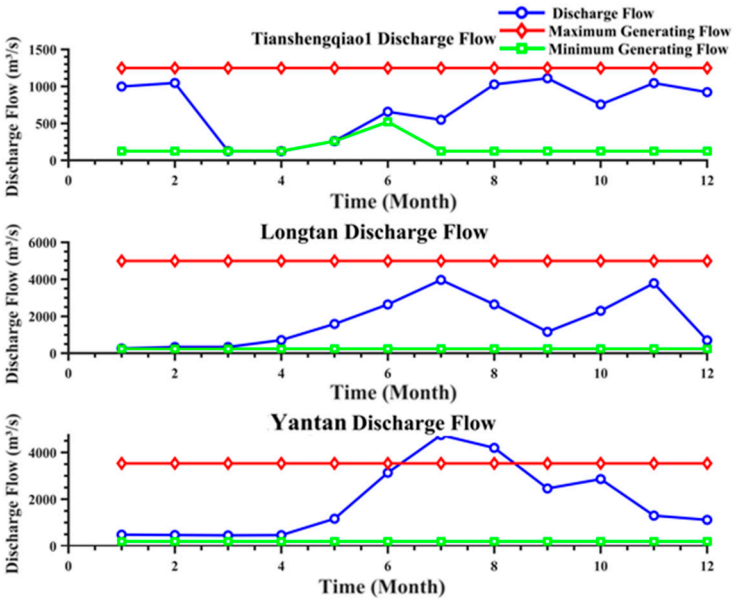


Figure 19. Discharge flow of each power station in multiple scenarios.

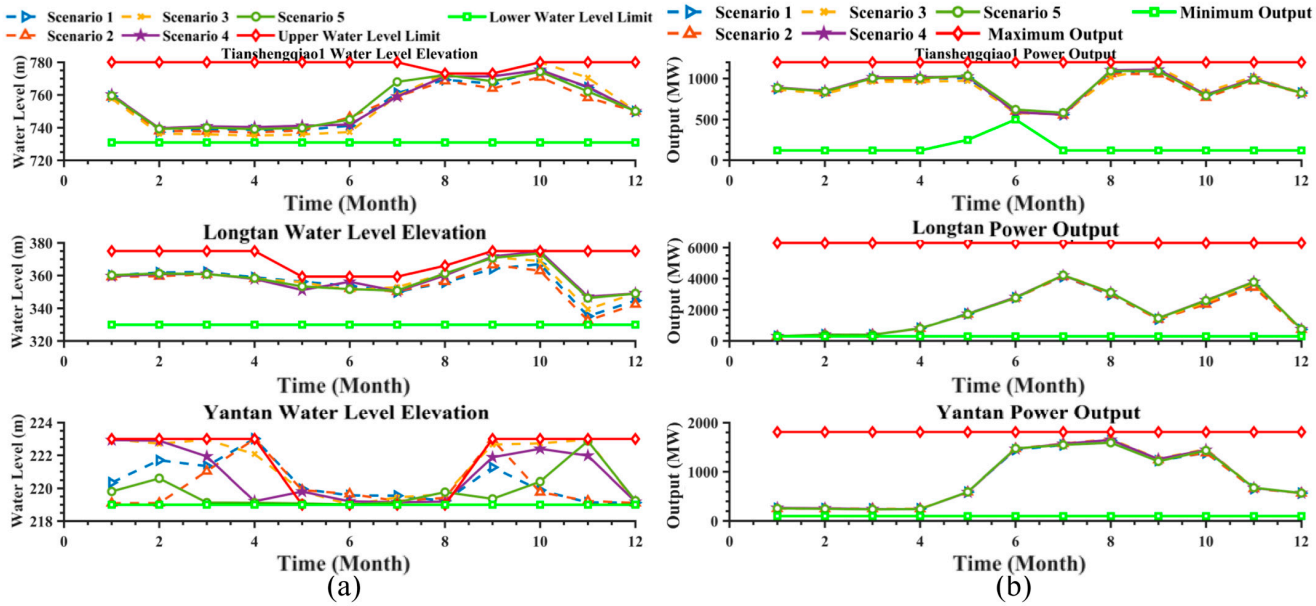


Figure 20. Water level, and power output of each power station in multiple scenarios: (**a**) water level variation curves and (**b**) power output variation curves.

The short-term output correction results for a certain scenario can be seen in Figure 21 (taking Yantan's 1st scenario as an example), with the correction results for different scenarios presented in a box plot illustrated in Figure 22. As shown in Figure 22, the differences in the correction results across scenarios are relatively small, which indicates that the short-term correction mechanism can effectively handle the fluctuations of different energy sources under various scenarios.

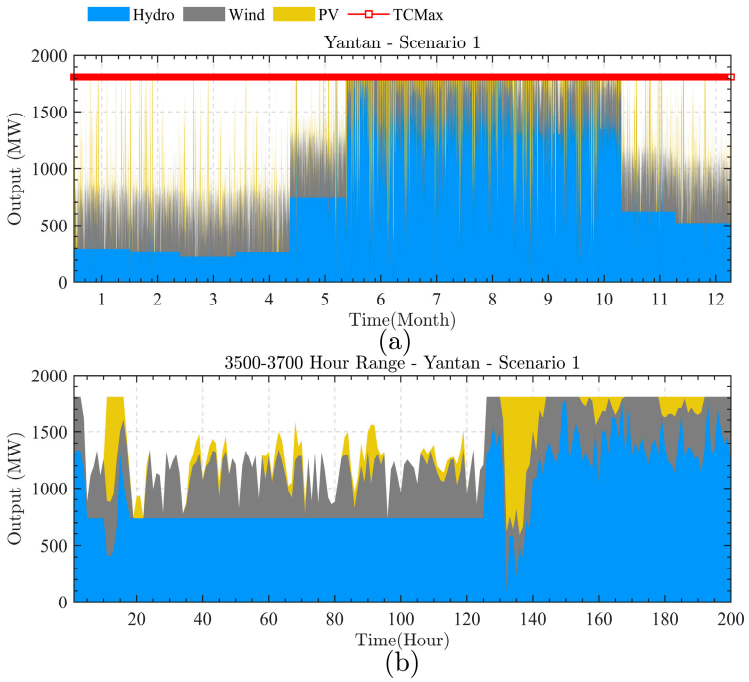


Figure 21. Short-term corrected hydro–wind–PV stacked power output chart for Yantan in a certain scenario: (**a**) stack plot shown by month and (**b**) local enlarged hourly stacking diagram.

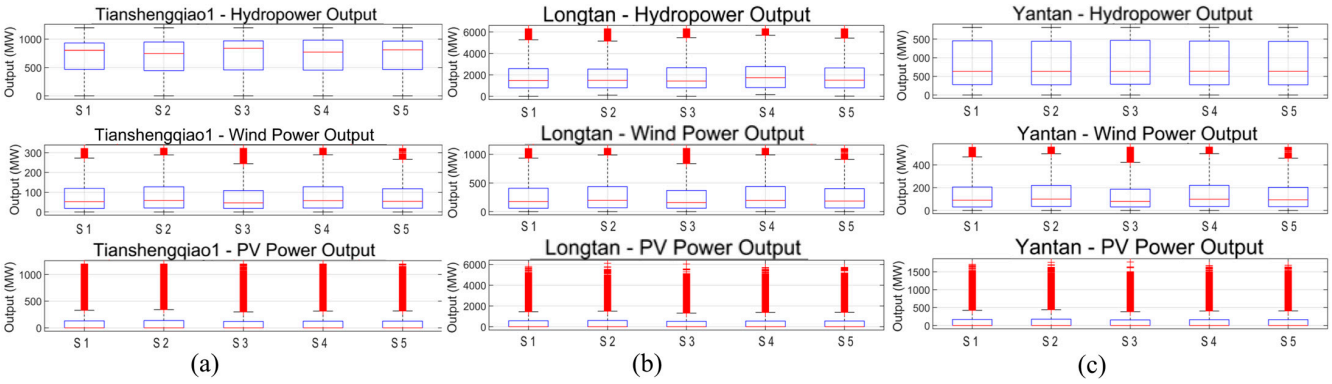


Figure 22. Short-term corrected hydro–wind–PV box plot for stations in multiple scenarios: (**a**) TianshengqiaoI, (**b**) Longtan and (**c**) Yantan.

For each power station, the median (red line) of the hydropower output across the five scenarios remains almost unchanged, showing that the corrected hydropower output is hardly affected by the changes in scenarios. The interquartile range (IQR) of the box plot is narrow, and the outliers are distributed within a reasonable range, indicating that the correction mechanism effectively balances the dynamic regulation needs of the reservoirs.

The box plots of both wind and PV power outputs indicate effective performance of the correction mechanism, with the wind power output showing little variation in distribution and almost identical median and IQR, suggesting strong robustness in handling

fluctuations. Similarly, the PV power output's small IQR and concentration of outliers near the upper limit further demonstrate the mechanism's efficacy in smoothing out short-term fluctuations. From the correction results, the stable output of hydropower provides a buffer for the fluctuations in wind and PV power, and the synergistic complementarity among the three energy sources is well demonstrated under the multi-scenario conditions.

Given that hydropower generation is inherently influenced by the seasonal variations in natural runoff, the hydropower stations adjust water discharge to achieve multi-energy complementary results. For example, during the wet season, when there is surplus regulated storage capacity of reservoirs, hydropower generation can be flexibly modulated to accommodate the output from wind and PV energy sources. Conversely, during dry seasons when the regulated storage capacity of reservoirs is constrained, hydropower deployments should adhere to principles of reservoir's storage. In this case, integration of renewable energy does not adversely impact the reservoir's storage strategy. The short-term output adjustment results fully utilize the complimentary characteristics of different energies, necessitating that the peaks and troughs in hydropower generation align with the troughs and peaks in total solar and wind power outputs. This alignment is crucial for achieving operational synergy among the three energy sources. Specifically, in the context of hydro–wind–PV complementarity, the scheduling strategy for cascade hydropower during dry seasons should reduce generation flow during periods of elevated wind and PV output, to ensure required reservoir water level. Conversely, when wind and PV output is diminished, the generation flow could be increased to boost hydropower output, thereby enhancing the overall total power generation during periods of low wind and PV availability.

5.4. Comparison and Analysis of Results from Different Algorithms

To evaluate the performance of the proposed EBORG algorithm, the results obtained by EBORG are compared with those obtained by the NSGA-II and standard Borg algorithm. NSGA-II is a widely used multi-objective optimization algorithm, which has been successfully applied in various multi-objective optimization problems [47,49]. It employs tournament selection, simulated binary crossover (SBX) [50], and polynomial mutation [51] to achieve the recombination process. By merging the parent and offspring populations and retaining the best-performing solutions in the merged population based on Pareto dominance ranking, NSGA-II ensures a good diversity of population and strong ability of Pareto front approximation.

To further compare the performance of different algorithms in 20 trials, the Coverage-metric (C-Metric) and Space-metric (S-Metric) [52] are used for evaluation. Specifically, C-Metric measures the dominance between two Pareto fronts, A and B, of a multi-objective problem. Let A and B be two Pareto fronts. The C-Metric, denoted as $C(A,\ B)$, is defined as the percentage of solutions in B that are dominated by at least one solution from A. This metric reflects the dominance relationship between the two sets and serves as an indicator to evaluate the quality of the Pareto solution set.

$$C(A,B) = \frac{|\{u \in B | \exists v \in A : v\ dominates\ u\}|}{|B|} \tag{23}$$

The numerator represents the number of solutions in B that are dominated by at least one solution from A; the denominator represents the total number of solutions in B. $C(A,B) = 1$ indicates that all solutions in B are dominated by some solutions in A, while $C(A,B) = 0$ indicates that no solution in B is dominated by any solution in A. Additionally, there is no equivalence between $C(A,B)$ and $1 - C(B,A)$.

For the S-Metric, consider a multi-objective optimization solution set $S = \{P_1, P_2, \ldots, P_n\}$, where each solution $P_i = (x_{i1}, x_{i2}, \ldots, x_{im})$ represents the coordinates in an m-dimensional objective space. The coordinates of each solution can be compared with a reference point $R = (r_1, r_2, \ldots, r_m)$ to compute the dominated volume.

For a solution P_i, the hyper-rectangle it generates can be defined, and its volume $V(P_i)$ is:

$$V(P_i) = \prod_{j=1}^{m} (r_j - x_{ij}) \tag{24}$$

where x_{ij} is the value of solution P_i in the j objective, and r_j is the value of the reference point R in the j objective. The volume $V(P_i)$ represents the hyper-rectangular volume formed by the spatial distances between the solution P_i and the reference point in each dimension. The total dominated volume $HV(S)$ of the multi-objective solution set S can be computed by summing the volumes of each solution and subtracting any overlapping areas. The formula for calculating the total dominated volume is typically expressed as:

$$HV(S) = \bigcup_{P_i \in S} V(P_i) \tag{25}$$

In this study, the C-Metric and S-Metric values were comparatively analyzed across different numbers of scenarios (1, 3, 5 and 8). As shown in Table 4, where Bt, Ag, and SD, respectively, denote the best domination rate, average domination rate, and standard deviation of domination rate, the proposed algorithm demonstrates consistently prominent performance metrics under varying scenario scales. Notably, its superior domination characteristics (evidenced by higher Bt and Ag values) coupled with lower standard deviation values across all test conditions confirm the algorithm's favorable robustness and scenario adaptability. A detailed introduction is provided for the test case with a scenario number of 5, where the execution times of different algorithms and the obtained Pareto front solutions are shown in Figure 23a and Figure 23b, respectively. It can be observed that the execution times of different algorithms do not differ significantly, and the Pareto fronts obtained by the BORG algorithm and NSGA-II algorithm are relatively close, with some overlapping solutions. However, the Pareto front obtained by the EBORG algorithm lies on the outer boundary of the others, indicating a significantly better performance. Additionally, the average domination rate of EBORG (C) over the NSGA-II (B) algorithm's Pareto front (i.e., the average value of $C(A, B)$) is approximately 84%, with $C(B, A)$ equal to 0. The comparison results between EBORG and BORG algorithms shows that $C(C, A)$ reaches 91%, with $C(A, C)$ equal to 0, indicating that the EBORG has the best domination performance. For the S-Metric values, $S(A)$ is superior to $S(C)$ and significantly better than $S(B)$, indicating that EBORG achieves the best convergence and solution diversity. Based on the fuzzy multiple attribute decision making method presented in [36], the final scheduling plan is selected based on the process of constructing indicators. The total power generation obtained by EBORG, BORG, and NSGA-II are 43,440,703.91 MWh, 42,217,661.99 MWh, and 42,327,349.93 MWh, respectively. It shows EBORG improves the result by 2.90% and 2.63%, compared with those obtained by BORG and NSGA-II. For the objective of maximizing the minimum output expectation, EBORG shows relative improvements of 1.23% and 0.96% compared to BORG and NSGA-II, respectively. Overall, the proposed algorithm demonstrates excellent performance in solving the optimization for the LHWP-CS problem. Regarding the changes in the objective function values under different number of scenarios, we conducted a comparative analysis of the expected total power generation and the expected average minimum output. Simulations with four typical scenario scales (1, 3, 5, and 8 scenarios) are performed, which correspond to expected total power generation values of 57,319,812.36 MWh, 49,603,186.25 MWh, 43,440,703.91 MWh, and

41,385,723.72 MWh, respectively, and expected average minimum outputs of 4528.36 MW, 3897.47 MW, 3257.31 MW, and 2941.87 MW. It was found that as the number of scenarios increased, both objectives show a gradual downward trend of change. This result effectively corroborates the management principles of diminishing returns under conservative decision-making tendencies and risk-reward trade-offs discussed in Section 5.3.2. This further validates that large-scale scenario simulations can better reflect the true risk characteristics of system operations. It also reveals the potential efficiency loss resulting from overly conservative dispatch strategies.

Table 4. Comparison of C-Metric and S-Metric values for BORG (A), NSGA-II (B), and EBORG (C) under different scenarios' size.

Combination	1			3			5			8		
	Bt	*Ag*	*SD*	*Bt*	*Ag*	*SD*	*Bt*	*Ag*	*SD*	*Bt*	*Ag*	*SD*
$C(C,A)$	1.00	0.98	0.01	1.00	0.94	0.02	1.00	0.91	0.02	1.00	0.91	0.03
$C(A,C)$	0.00	0.00	0.00	0.00	0.00	0.00	0.00	0.00	0.00	0.00	0.00	0.00
$C(B,C)$	0.00	0.00	0.00	0.00	0.00	0.00	0.00	0.00	0.00	0.00	0.00	0.00
$C(C,B)$	1.00	0.96	0.01	1.00	0.88	0.02	1.00	0.84	0.03	1.00	0.81	0.05
$S(A)$	2.35×10^9	7.65×10^8	5.69×10^7	1.96×10^9	4.52×10^8	4.51×10^7	1.22×10^9	3.72×10^8	3.11×10^7	1.01×10^9	2.85×10^8	2.71×10^7
$S(B)$	7.53×10^8	4.56×10^8	2.19×10^7	7.21×10^8	4.03×10^8	1.68×10^7	6.38×10^8	3.01×10^8	1.31×10^7	4.68×10^8	2.04×10^8	1.03×10^7
$S(C)$	1.94×10^9	8.36×10^8	4.21×10^7	1.57×10^9	7.36×10^8	3.46×10^7	1.11×10^9	6.12×10^8	2.11×10^7	8.63×10^8	2.35×10^8	2.08×10^7

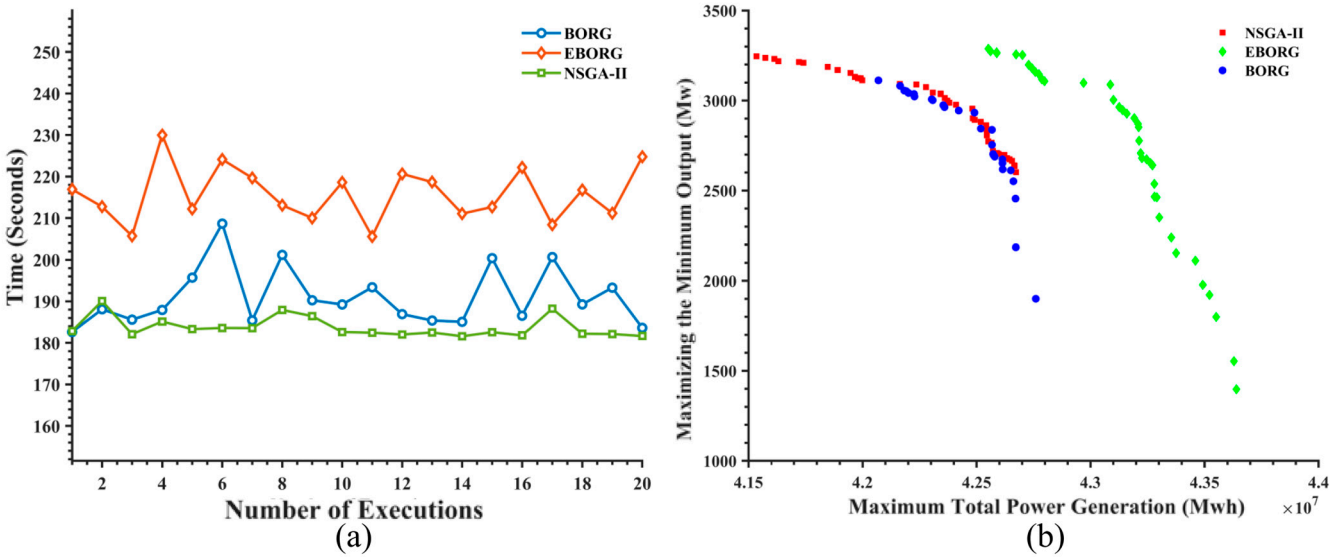


Figure 23. Comparison of execution times for different algorithms (**a**) and comparison of Pareto fronts obtained from different algorithms (**b**).

Previous discussions have highlighted the evident advantages of the evolutionary multi-objective optimization method proposed in this paper over traditional optimization methods. To further investigate the impact of different recombination operators and the two distinct dominance rules on the final optimization outcomes, the operational results were examined by systematically removing each operator under a five-scenario scale. Additionally, we removed the ε-box dominance rule from the algorithm and maintain the Pareto dominance rule, and the solutions obtained are also illustrated in Figure 24. We can see that removal of any operator leads to a performance degradation of algorithm. Meanwhile, removing the ε-box dominance rule from the algorithm also undermines the performance of the algorithm in solving the problem. The results suggest a significant influence of each recombination operator and the two different dominance rules on the performances of the proposed algorithm.

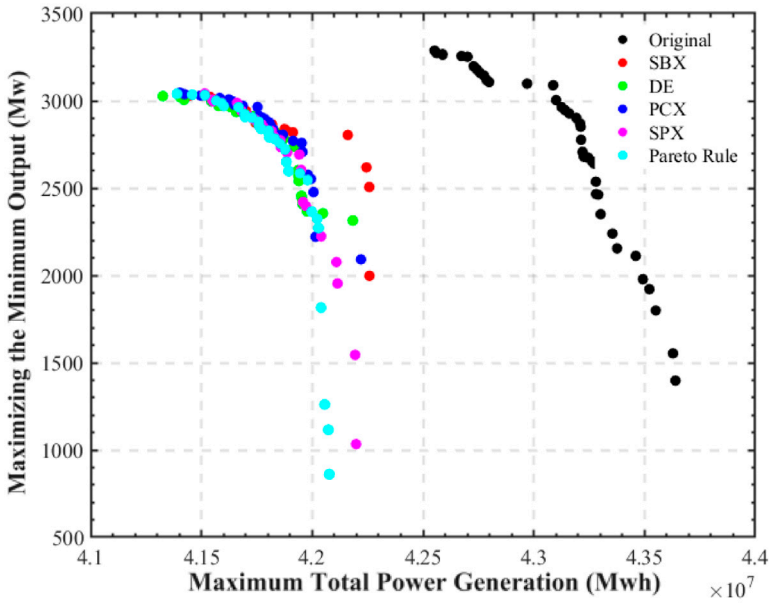


Figure 24. Effects of different operators and dominance rules on the resulting Pareto front.

6. Conclusions

This study addresses the issue of multiple uncertainties associated with hydro, wind, and PV resources of LHWP-CS. Markov chains and Copula functions are integrated to quantify the correlations between runoff, wind power and PV power. A vast array of scenarios are generated based on the established correlations and the number of scenarios is then reduced to a manageable scale through a probabilistic distance-based technique. A comprehensive long-term multi-objective stochastic scheduling optimization model is proposed for the LHWP-CS problem, aiming at maximizing the expected total power generation of the entire scheduling period and expected minimum output in each period. Due to the NP-hard nature of the problem, an innovative EBORG algorithm with tailored constraint handling strategies is introduced. Furthermore, a short-term output correction mechanism is proposed to refine the long-term scheduling theme. Finally, experiments on three annual regulation reservoirs in Hongshui River Basin are conducted to verify the functionality of the proposed model and algorithm.

The results of this study demonstrate the effectiveness of the proposed methods in addressing the multiple uncertainties associated with hydro, wind, and PV resources in the LHWP-CS. The established time correlation model and resource correlation model effectively capture the uncertainty features of these renewable energy sources, providing an accurate representation of their interdependencies. The results obtained in a single scenario underscore the feasibility of the multi-objective stochastic scheduling optimization model for LHWP-CS. The proposed EBORG algorithm with tailored constraint handling strategies efficiently solves the model. Compared with the BORG and NSGA-II algorithms, EBORG exhibits significant advantages in terms of domination rate and convergence, with improvements of 2.90% and 2.63% in total power generation, respectively. Additionally, the number of scenarios is found to play a crucial role in balancing the tradeoff between economic performance and risk management for the LHWP-CS, where decision-makers must carefully select the optimal number of scenarios to balance risk and reward according to practical requirements. The proposed short-term output correction mechanism proposed in this study effectively refines long-term scheduling output plans by leveraging the complementarity of hydro, wind, and PV resources.

This study opens several directions for future research on LHWP-CS. One promising direction is the extension of the model to incorporate daily operational risks and peak-

shaving capabilities during the long-term multi-energy complementary scheduling process. To achieve this, a multi-scale model integrating both long-term and short-term scheduling could be developed, although this approach would come with substantial computational burdens. As a result, specific algorithms to address this challenge will be crucial for further advancements in this field. In addition, some important factors that may exist in practice but have not been considered in this study, such as market price volatility [26], fluctuations in power demand, and influence of social policies, can be further extended to enhance the comprehensiveness and applicability of the research results.

Author Contributions: Conceptualization, B.J.; Data curation, H.H., C.C. and Z.Z.; Formal analysis, H.H., F.Z., J.G. and S.S.Y.; Funding acquisition, B.J. and Z.Z.; Investigation, B.J. and H.H.; Methodology, B.J. and H.H.; Project administration, B.J., J.G. and Z.Z.; Resources, B.J., C.C. and Z.Z.; Software, B.J., H.H. and Y.G.; Supervision, B.J. and F.Z.; Validation, H.H., Y.G. and Z.Z.; Visualization, H.H. and Y.G.; Writing—original draft, B.J., H.H. and Y.G.; Writing—review and editing, B.J., H.H., Y.G., J.G. and S.S.Y. All authors have read and agreed to the published version of the manuscript.

Funding: This research was funded by the project (No. ZXGN-KW2406-007) supported by China Water Resources and Hydropower Construction Engineering Consulting Co., Ltd.

Institutional Review Board Statement: Not applicable.

Informed Consent Statement: Not applicable.

Data Availability Statement: The data presented in this study are available on request from the corresponding author.

Acknowledgments: We would like to thank the editors and the anonymous reviewers for their constructive suggestions.

Conflicts of Interest: Zenghai Zhao was employed by the China Water Resources and Hydropower Construction Engineering Consulting Co., LTD. The remaining authors declare that the research was conducted in the absence of any commercial or financial relationships that could be construed as a potential conflict of interest.

References

1. Lei, K.; Chang, J.; Wang, X.; Guo, A.; Wang, Y.; Ren, C. Peak Shaving and Short-Term Economic Operation of Hydro-Wind-PV Hybrid System Considering the Uncertainty of Wind and PV Power. *Renew. Energy* **2023**, *215*, 118903. [CrossRef]
2. Chen, C.; Liu, H.; Xiao, Y.; Zhu, F.; Ding, L.; Yang, F. Power Generation Scheduling for a Hydro-Wind-Solar Hybrid System: A Systematic Survey and Prospect. *Energies* **2022**, *15*, 8747. [CrossRef]
3. Psarros, G.N.; Papathanassiou, S.A. Generation Scheduling in Island Systems with Variable Renewable Energy Sources: A Literature Review. *Renew. Energy* **2023**, *205*, 1105–1124. [CrossRef]
4. Xiong, H.; Egusquiza, M.; Alberg Østergaard, P.; Pérez-Díaz, J.I.; Sun, G.; Egusquiza, E.; Patelli, E.; Xu, B.; Duan, H.; Chen, D.; et al. Multi-Objective Optimization of a Hydro-Wind-Photovoltaic Power Complementary Plant with a Vibration Avoidance Strategy. *Appl. Energy* **2021**, *301*, 117459. [CrossRef]
5. Han, B.; Zahraoui, Y.; Mubin, M.; Mekhilef, S.; Seyedmahmoudian, M.; Stojcevski, A. Home Energy Management Systems: A Review of the Concept, Architecture, and Scheduling Strategies. *IEEE Access* **2023**, *11*, 19999–20025. [CrossRef]
6. Balan, M.H.; Camargo, L.A.S.; Ramos, D.S.; Castro, R.; Leonel, L.D.; Pulcherio, E.S.; Melendez, J. Hydro–Solar Hybrid Plant Operation in a Hydropower Plant Cascade: Optimizing Local and Bulk System Benefits. *Water* **2024**, *16*, 2053. [CrossRef]
7. Xie, T.; Zhang, C.; Wang, T.; Cao, W.; Shen, C.; Wen, X.; Mao, C. Optimization and Service Lifetime Prediction of Hydro-Wind Power Complementary System. *J. Clean Prod.* **2021**, *291*, 125983. [CrossRef]
8. Ren, Y.; Yao, X.; Liu, D.; Qiao, R.; Zhang, L.; Zhang, K.; Jin, K.; Li, H.; Ran, Y.; Li, F. Optimal Design of Hydro-Wind-PV Multi-Energy Complementary Systems Considering Smooth Power Output. *Sustain. Energy Technol. Assess.* **2022**, *50*, 101832. [CrossRef]
9. Tian, Y.; Chang, J.; Wang, Y.; Wang, X.; Meng, X.; Guo, A. The Capacity Planning Method for a Hydro-Wind-PV-Battery Complementary System Considering the Characteristics of Multi-Energy Integration into Power Grid. *J. Clean. Prod.* **2024**, *446*, 141292. [CrossRef]

10. Wang, S.; Jia, R.; Luo, C.; An, Y.; Guo, P. Spatiotemporal Complementary Characteristics of Large-Scale Wind Power, Photovoltaic Power, and Hydropower. *Sustainability* **2022**, *14*, 9273. [CrossRef]
11. Tan, Q.; Zhang, Z.; Wen, X.; Fang, G.; Xu, S.; Nie, Z.; Wang, Y. Risk Control of Hydropower-Photovoltaic Multi-Energy Complementary Scheduling Based on Energy Storage Allocation. *Appl. Energy* **2024**, *358*, 122610. [CrossRef]
12. Wang, X.; Chang, J.; Meng, X.; Wang, Y. Short-Term Hydro-Thermal-Wind-Photovoltaic Complementary Operation of Interconnected Power Systems. *Appl. Energy* **2018**, *229*, 945–962. [CrossRef]
13. Li, F.; Chen, S.; Ju, C.; Zhang, X.; Ma, G.; Huang, W. Research on Short-Term Joint Optimization Scheduling Strategy for Hydro-Wind-Solar Hybrid Systems Considering Uncertainty in Renewable Energy Generation. *Energy Strategy Rev.* **2023**, *50*, 101242. [CrossRef]
14. Wang, H.; Liao, S.; Cheng, C.; Liu, B.; Fang, Z.; Wu, H. Short-Term Scheduling Strategies for Hydro-Wind-Solar-Storage Considering Variable-Speed Unit of Pumped Storage. *Appl. Energy* **2025**, *377*, 124336. [CrossRef]
15. Zhang, J.; Wang, H.; Fan, C.; Hu, J.; Zhang, X. Hydro–Wind–PV–Integrated Operation Optimization and Ultra-Short-Term HESS Configuration. *Electronics* **2024**, *13*, 4778. [CrossRef]
16. Pedruzzi, R.; Silva, A.R.; Soares dos Santos, T.; Araujo, A.C.; Cotta Weyll, A.L.; Lago Kitagawa, Y.K.; Nunes da Silva Ramos, D.; Milani de Souza, F.; Almeida Narciso, M.V.; Saraiva Araujo, M.L.; et al. Review of Mapping Analysis and Complementarity between Solar and Wind Energy Sources. *Energy* **2023**, *283*, 129045. [CrossRef]
17. Jia, H.; Li, H.; Zhang, Z.; Sun, W. Complementary Analysis and Performance Improvement of a Hydro-Wind Hybrid Power System. *Water* **2024**, *16*, 2912. [CrossRef]
18. Cheng, Q.; Liu, P.; Ming, B.; Yang, Z.; Cheng, L.; Liu, Z.; Huang, K.; Xu, W.; Gong, L. Synchronizing Short-, Mid-, and Long-Term Operations of Hydro-Wind-Photovoltaic Complementary Systems. *Energy* **2024**, *305*, 132309. [CrossRef]
19. Lu, L.; Yuan, W.; Xu, H.; Su, C.; Yan, D.; Wu, Z. Evaluation of the Complementary Characteristics for Wind-Photovoltaic-Hydro Hybrid System Considering Multiple Uncertainties in the Medium and Long Term. *Water Resour. Manag.* **2024**, *38*, 793–814. [CrossRef]
20. Camal, S.; Teng, F.; Michiorri, A.; Kariniotakis, G.; Badesa, L. Scenario Generation of Aggregated Wind, Photovoltaics and Small Hydro Production for Power Systems Applications. *Appl. Energy* **2019**, *242*, 1396–1406. [CrossRef]
21. Ming, B.; Chen, J.; Fang, W.; Liu, P.; Zhang, W.; Jiang, J. Evaluation of Stochastic Optimal Operation Models for Hydro–Photovoltaic Hybrid Generation Systems. *Energy* **2023**, *267*, 126500. [CrossRef]
22. Lu, N.; Wang, G.; Su, C.; Ren, Z.; Peng, X.; Sui, Q. Medium- and Long-Term Interval Optimal Scheduling of Cascade Hydropower-Photovoltaic Complementary Systems Considering Multiple Uncertainties. *Appl. Energy* **2024**, *353*, 122085. [CrossRef]
23. Li, Z.; Yang, P.; Guo, Y.; Lu, G. Medium-Term Multi-Stage Distributionally Robust Scheduling of Hydro–Wind–Solar Complementary Systems in Electricity Markets Considering Multiple Time-Scale Uncertainties. *Appl. Energy* **2023**, *347*, 121371. [CrossRef]
24. Ding, Z.; Wen, X.; Tan, Q.; Yang, T.; Fang, G.; Lei, X.; Zhang, Y.; Wang, H. A Forecast-Driven Decision-Making Model for Long-Term Operation of a Hydro-Wind-Photovoltaic Hybrid System. *Appl. Energy* **2021**, *291*, 116820. [CrossRef]
25. Xu, S.; Liu, P.; Li, X.; Cheng, Q.; Liu, Z. Deriving Long-Term Operating Rules of the Hydro-Wind-PV Hybrid Energy System Considering Electricity Price. *Renew. Energy* **2023**, *219*, 119353. [CrossRef]
26. Zhang, H.; Li, Z.; Xue, Y.; Chang, X.; Su, J.; Wang, P.; Guo, Q.; Sun, H. A Stochastic Bi-Level Optimal Allocation Approach of Intelligent Buildings Considering Energy Storage Sharing Services. *IEEE Trans. Consum. Electron.* **2024**, *70*, 5142–5153. [CrossRef]
27. Zhou, S.; Han, Y.; Zalhaf, A.S.; Chen, S.; Zhou, T.; Yang, P.; Elboshy, B. A Novel Multi-Objective Scheduling Model for Grid-Connected Hydro-Wind-PV-Battery Complementary System under Extreme Weather: A Case Study of Sichuan, China. *Renew. Energy* **2023**, *212*, 818–833. [CrossRef]
28. Li, H.; Liu, P.; Guo, S.; Ming, B.; Cheng, L.; Yang, Z. Long-Term Complementary Operation of a Large-Scale Hydro-Photovoltaic Hybrid Power Plant Using Explicit Stochastic Optimization. *Appl. Energy* **2019**, *238*, 863–875. [CrossRef]
29. Wang, F.; Xu, J.; Wang, Q. Complementary Operation Based Sizing and Scheduling Strategy for Hybrid Hydro-PV-Wind Generation Systems Connected to Long-Distance Transmission Lines. *Appl. Energy* **2024**, *364*, 123082. [CrossRef]
30. Lei, H.; Liu, P.; Cheng, Q.; Xu, H.; Liu, W.; Zheng, Y.; Chen, X.; Zhou, Y. Frequency, Duration, Severity of Energy Drought and Its Propagation in Hydro-Wind-Photovoltaic Complementary Systems. *Renew. Energy* **2024**, *230*, 120845. [CrossRef]
31. Shen, Q.; Mo, L.; Liu, Z.; Sun, X.; Liu, G.; Zhang, Y. A Multi-Objective Optimization Method of Sustainable Wind–Photovoltaic–Hydro Systems Considering Source–Grid Coordination. *Sustainability* **2024**, *16*, 61. [CrossRef]
32. Zhai, X.; Li, Z.; Li, Z.; Xue, Y.; Chang, X.; Su, J.; Jin, X.; Wang, P.; Sun, H. Risk-Averse Energy Management for Integrated Electricity and Heat Systems Considering Building Heating Vertical Imbalance: An Asynchronous Decentralized Approach. *Appl. Energy* **2025**, *383*, 125271. [CrossRef]
33. Evans, G.W. An Overview of Techniques for Solving Multiobjective Mathematical Programs. *Manag. Sci.* **1984**. [CrossRef]
34. Zhou, S.; Ji, B.; Song, Y.; Yu, S.S.; Zhang, D.; Van Woensel, T. Hub-and-Spoke Network Design for Container Shipping in Inland Waterways. *Expert Syst. Appl.* **2023**, *223*, 119850. [CrossRef]

35. Ji, B.; Zhang, D.; Zhang, Z.; Yu, S.S.; Van Woensel, T. The Generalized Serial-Lock Scheduling Problem on Inland Waterway: A Novel Decomposition-Based Solution Framework and Efficient Heuristic Approach. *Transp. Res. Part E Logist. Transp. Rev.* **2022**, *168*, 102935. [CrossRef]
36. Ji, B.; Yuan, X.; Chen, Z.; Tian, H. Improved Gravitational Search Algorithm for Unit Commitment Considering Uncertainty of Wind Power. *Energy* **2014**, *67*, 52–62. [CrossRef]
37. Shumway, R.H.; Stoffer, D.S. (Eds.) ARIMA Models. In *Time Series Analysis and Its Applications: With R Examples*; Springer International Publishing: Cham, Switzerland, 2017; pp. 75–163, ISBN 978-3-319-52452-8.
38. Wang, W.; Dong, Z.; Si, W.; Zhang, Y.; Xu, W. Two-Dimension Monthly River Flow Simulation Using Hierarchical Network-Copula Conditional Models. *Water Resour. Manag.* **2018**, *32*, 3801–3820. [CrossRef]
39. Zhang, H.; Lu, Z.; Hu, W.; Wang, Y.; Dong, L.; Zhang, J. Coordinated Optimal Operation of Hydro–Wind–Solar Integrated Systems. *Appl. Energy* **2019**, *242*, 883–896. [CrossRef]
40. Montes-Iturrizaga, R.; Heredia-Zavoni, E. Multivariate Environmental Contours Using C-Vine Copulas. *Ocean Eng.* **2016**, *118*, 68–82. [CrossRef]
41. Dong, W.; Sun, H.; Tan, J.; Li, Z.; Zhang, J.; Yang, H. Regional Wind Power Probabilistic Forecasting Based on an Improved Kernel Density Estimation, Regular Vine Copulas, and Ensemble Learning. *Energy* **2022**, *238*, 122045. [CrossRef]
42. Du, E.; Zhang, N.; Kang, C.; Bai, J.; Cheng, L.; Ding, Y. Impact of Wind Power Scenario Reduction Techniques on Stochastic Unit Commitment. In Proceedings of the 2016 Second International Symposium on Stochastic Models in Reliability Engineering, Life Science and Operations Management (SMRLO), Beer Sheva, Israel, 15–18 February 2016; pp. 202–210.
43. Chen, Y.; Wei, W.; Liu, F.; Mei, S. Distributionally Robust Hydro-Thermal-Wind Economic Dispatch. *Appl. Energy* **2016**, *173*, 511–519. [CrossRef]
44. Hadka, D.; Reed, P. Borg: An Auto-Adaptive Many-Objective Evolutionary Computing Framework. *Evol. Comput.* **2013**, *21*, 231–259. [CrossRef]
45. Ji, B.; Zhang, B.; Yu, S.S.; Zhang, D.; Yuan, X. An Enhanced Borg Algorithmic Framework for Solving the Hydro-Thermal-Wind Co-Scheduling Problem. *Energy* **2021**, *218*, 119512. [CrossRef]
46. Vrugt, J.A.; Robinson, B.A. Improved Evolutionary Optimization from Genetically Adaptive Multimethod Search. *Proc. Natl. Acad. Sci. USA* **2007**, *104*, 708–711. [CrossRef] [PubMed]
47. Deb, K.; Pratap, A.; Agarwal, S.; Meyarivan, T. A Fast and Elitist Multiobjective Genetic Algorithm: NSGA-II. *IEEE Trans. Evol. Comput.* **2002**, *6*, 182–197. [CrossRef]
48. Yuan, X.; Tian, H.; Yuan, Y.; Huang, Y.; Ikram, R.M. An Extended NSGA-III for Solution Multi-Objective Hydro-Thermal-Wind Scheduling Considering Wind Power Cost. *Energy Conv. Manag.* **2015**, *96*, 568–578. [CrossRef]
49. Ji, B.; Huang, H.; Yu, S.S. An Enhanced NSGA-II for Solving Berth Allocation and Quay Crane Assignment Problem With Stochastic Arrival Times. *IEEE Trans. Intell. Transp. Syst.* **2023**, *24*, 459–473. [CrossRef]
50. Chacón, J.; Segura, C. Analysis and Enhancement of Simulated Binary Crossover. In Proceedings of the 2018 IEEE Congress on Evolutionary Computation (CEC), Rio de Janeiro, Brazil, 8–13 July 2018; pp. 1–8.
51. Carles-Bou, J.L.; Galán, S.F. Self-Adaptive Polynomial Mutation in NSGA-II. *Soft Comput.* **2023**, *27*, 17711–17727. [CrossRef]
52. Audet, C.; Bigeon, J.; Cartier, D.; Le Digabel, S.; Salomon, L. Performance Indicators in Multiobjective Optimization. *Eur. J. Oper. Res.* **2021**, *292*, 397–422. [CrossRef]

Disclaimer/Publisher's Note: The statements, opinions and data contained in all publications are solely those of the individual author(s) and contributor(s) and not of MDPI and/or the editor(s). MDPI and/or the editor(s) disclaim responsibility for any injury to people or property resulting from any ideas, methods, instructions or products referred to in the content.